

AD-A216 214

DTIC FILE COPY

2

College of Earth and Mineral Sciences

PENNSYLVANIA STATE UNIVERSITY



DTIC
ELECTE
DEC 27 1989
S D

DEPARTMENT OF MATERIALS SCIENCE
METALLURGY PROGRAM

TECHNICAL REPORT

December 1989

Contract No. N00014-84-k-0201

HYDROGEN SULFIDE EFFECT ON HYDROGEN ENTRY INTO IRON
- A MECHANISTIC STUDY

H. W. Pickering

Department of Materials Science and Engineering
The Pennsylvania State University

DISTRIBUTION STATEMENT A
Approved for public release
Distribution Unlimited

89 12 21 019

PENN STATE

College of Earth and Mineral Sciences

Undergraduate Majors

Ceramic Science and Engineering, Fuel Science, Metals Science and Engineering, Polymer Science, Mineral Economics; Mining Engineering, Petroleum and Natural Gas Engineering; Earth Sciences, Geosciences: Geography; Meteorology.

Graduate Programs and Fields of Research

Ceramic Science and Engineering, Fuel Science, Metals Science and Engineering, Polymer Science, Mineral Economics, Mining Engineering, Mineral Processing, Petroleum and Natural Gas Engineering; Geochemistry and Mineralogy, Geology, Geophysics; Geography; Meteorology.

Universitywide Interdisciplinary Graduate Programs Involving EMS Faculty and Students

Earth Sciences, Ecology, Environmental Pollution Control Engineering, Mineral Engineering Management, Solid State Science.

Associate Degree Programs

Metallurgical Engineering Technology (Shenango Valley Campus).

Interdisciplinary Research Groups Centered in the College

C. Drew Stahl Center for Advanced Oil Recovery, Center for Advanced Materials, Coal Research Section, Earth System Science Center, Mining and Mineral Resources Research Institute, Ore Deposits Research Group.

Analytical and Characterization Laboratories (Mineral Constitution Laboratories)

Services available include: classical chemical analysis of metals and silicate and carbonate rocks, X-ray diffraction and fluorescence, electron microscopy and diffraction, electron microprobe analysis, atomic absorption analysis, spectrochemical analysis, surface analysis by secondary ion mass spectrometry (SIMS); and scanning electron microscopy (SEM).

The Pennsylvania State University, in compliance with federal and state laws, is committed to the policy that all persons shall have equal access to programs, admission, and employment without regard to race, religion, sex, national origin, handicap, age, or status as a disabled or Vietnam-era veteran. Direct all affirmative action inquiries to the Affirmative Action Officer, Suzanne Brooks, 201 Willard Building, University Park, PA 16802; (814) 863-0471.
U.Ed. 87-1027

Produced by the Penn State Department of Publications

REPORT DOCUMENTATION PAGE

Form Approved
GSA No. 0704-0128

1a. REPORT SECURITY CLASSIFICATION NONE		1b. RESTRICTIVE MARKINGS	
2a. SECURITY CLASSIFICATION AUTHORITY		3. DISTRIBUTION/AVAILABILITY OF REPORT	
2b. DECLASSIFICATION/DOWNGRADING SCHEDULE			
4. PERFORMING ORGANIZATION REPORT NUMBER(S)		5. MONITORING ORGANIZATION REPORT NUMBER(S)	
6a. NAME OF PERFORMING ORGANIZATION Howard W. Pickering	6b. OFFICE SYMBOL (If applicable)	7a. NAME OF MONITORING ORGANIZATION Office of Naval Research	
6c. ADDRESS (City, State, and ZIP Code) The Pennsylvania State University University Park, PA 16802		7b. ADDRESS (City, State, and ZIP Code) Arlington, VA 22217	
8a. NAME OF FUNDING/SPONSORING ORGANIZATION	8b. OFFICE SYMBOL (If applicable)	9. PROCUREMENT INSTRUMENT IDENTIFICATION NUMBER	
8c. ADDRESS (City, State, and ZIP Code)		10. SOURCE OF FUNDING NUMBERS	
		PROGRAM ELEMENT NO. 84-K-0201	PROJECT NO. 4315098
		TASK NO.	WORK UNIT ACCESSION NO.
11. TITLE (Include Security Classification) "Hydrogen Sulfide Effect on Hydrogen Entry Into Iron - A Mechanistic Study"			
12. PERSONAL AUTHOR(S) Pickering, Howard W.			
13a. TYPE OF REPORT Interim	13b. TIME COVERED FROM 12/15/88 TO 12/14/89	14. DATE OF REPORT (Year, Month, Day) 1989 December	15. PAGE COUNT 42
16. SUPPLEMENTARY NOTATION K 11			
17. COLAB CODES		18. SUBJECT TERMS (Continue on reverse if necessary and identify by block number)	
FIELD	GROUP	SUB-GROUP	
		Hydrogen charging in iron; H ₂ S effect in acids on: surface H coverage, entry and overpotential; h.e.r., absorption and adsorption rate constants; modified I-P-Z model.	
19. ABSTRACT (Continue on reverse if necessary and identify by block number) The recently developed I-P-Z model is modified in order to analyze the observed enhanced permeation of hydrogen that occurs in the presence of hydrogen sulfide during cathodic hydrogen charging of iron. The modification accounts for the fact that the energy of adsorption becomes coverage dependent at the higher coverages and affects the hydrogen evolution reaction (h.e.r.) in the presence of H ₂ S. Charging experiments were performed on Ferrovac E-Iron membranes 0.5mm thick using a Deyanathan-Stachurski cell in deaerated, pre-electrolyzed solutions made from 0.1M HClO ₄ and 0.1M NaClO ₄ with pH values of 1 and 2. The transfer coefficient, α , exchange current density, i_0 , thickness-dependent absorption-adsorption rate constant, k , recombination rate constant, k_3 , surface hydrogen coverage, θ_H , and discharge rate constant, k_d , were obtained by application of the model to the experimental results. As a result, the role of H ₂ S has been modified. While θ_H is increased in the presence of H ₂ S, the overpotential, η , is decreased consistent with an observed increase in α , and the increased H entry is found to be the result of a decreased k_3 as well as the increased α . In addition, a very important relationship has been derived that will enable the calculation of the absorption, k_{abs} , and adsorption, k_{ads} , rate constants from the electrochemical permeation results for different membrane thicknesses.			
20. DISTRIBUTION/AVAILABILITY OF ABSTRACT <input checked="" type="checkbox"/> UNCLASSIFIED/UNLIMITED <input type="checkbox"/> SAME AS RPT <input type="checkbox"/> DTIC USERS		21. ABSTRACT SECURITY CLASSIFICATION	
22a. NAME OF RESPONSIBLE INDIVIDUAL A. J. Sedrik		22b. TELEPHONE (Include Area Code) (202) 696-4401	22c. OFFICE SYMBOL 1131M

etc

5. code

-5003

11/11/89

HYDROGEN SULFIDE EFFECT ON HYDROGEN ENTRY INTO IRON - A MECHANISTIC STUDY

Rajan N. Iyer, Izumi Takeuchi*, Mehrooz Zamanzadeh** and
Howard W. Pickering

Department of Materials Science and Engineering
The Pennsylvania State University
University Park, PA 16802

ABSTRACT

The recently developed I-P-Z model is modified in order to analyze the observed enhanced permeation of hydrogen that occurs in the presence of hydrogen sulfide during cathodic hydrogen charging of iron. The modification accounts for the fact that the energy of adsorption becomes coverage dependent at the higher coverages and affects the hydrogen evolution reaction (h.e.r.) in the presence of H_2S . Charging experiments were performed on Ferrovac E-Iron membranes 0.5 mm thick using a Devanathan-Stachurski cell in deaerated, pre-electrolyzed solutions made from 0.1M $HClO_4$ and 0.1M $NaClO_4$ with pH values of 1 and 2. The transfer coefficient, α , exchange current density, i_0 , thickness-dependent absorption-adsorption rate constant, k'' , recombination rate constant, k_3 , surface hydrogen coverage, θ_H , and discharge rate constant, k_p^0 , were obtained by application of the model to the experimental results. As a result, the role of H_2S has been clarified. While θ_H is increased in the presence of H_2S , the overpotential, η , is decreased consistent with an observed increase in α , and the increased H entry is found to be the result of a decreased k_3 as well as the increased α . In addition, a very important relationship has been derived that will enable the calculation of the absorption, k_{abs} , and adsorption, k_{ads} , rate constants from the electrochemical permeation results for different membrane thicknesses.

* Present address: Kashima Steel Works, Sumitomo Metals Industries, Ltd., Kashima, Japan.

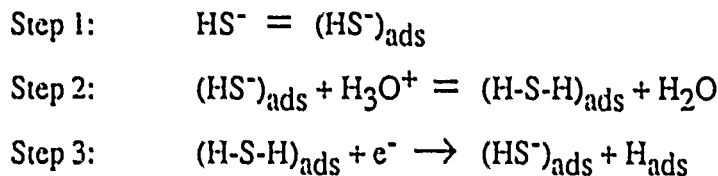
** Present address: Professional Services Industries - P T L Division, 850 Poplar Street, Pittsburgh, PA 15220.

INTRODUCTION

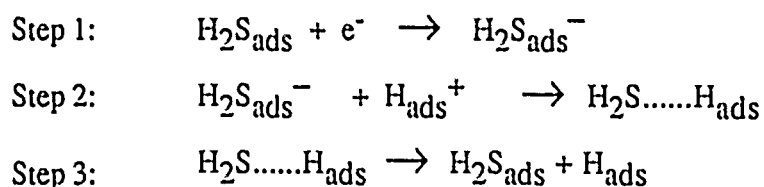
Since the failure of steels in wet hydrogen sulfide (H_2S) is well known to occur in many technological situations, especially in oil and gas field applications ⁽¹⁾, many studies have been carried out in order to better define and understand this problem. It is well known that in the presence of H_2S , the concentration of hydrogen in steels is increased sharply ⁽¹⁻⁶⁾. It is also now generally accepted that when the concentration of hydrogen in a metal reaches a critical level, cracking can occur ⁽⁷⁾.

It has often been suggested ⁽⁶⁾, based on a measured increase in hydrogen uptake, that H_2S has a "poisoning" effect on the hydrogen evolution reaction (h.e.r.). Contrary arguments based on polarization and permeation experiments have provided different mechanisms ^(3,4,5,8) for the role of H_2S in the entry of hydrogen into iron and steel. There is also a mechanistic dilemma on the significant effect that H_2S has on the kinetics of the h.e.r. and hence on hydrogen absorption.

There are at least four main proposals of the mechanism of the enhancement of hydrogen absorption by iron due to H_2S . The first of these, which was developed by Iofa and Kam ⁽⁸⁾ considers the following sequence of reactions:



In this model, steps (1) and (2) are quasi-reversible and step (3) is considered to be rate limiting. On the basis of their experimental data in 0.1N H_2SO_4 , Iofa and Kam concluded that the HS^- anion accelerates the discharge of H^+ ion. However, their interpretations were incomplete in the sense that the reaction parameters remained unknown and in fact, there is a far higher concentration of H_2S compared to HS^- in acid solutions ⁽⁹⁾, as shown in Figure 1. So, Kawashima et al ⁽³⁾ proposed the following reaction sequence:

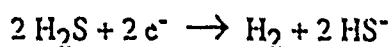


	Approved by _____ Date _____ _____ _____
A-1	

They showed that H_2S did not change the Tafel slope, but did decrease the cathodic overpotential in acid solutions. In their model, H_2S works as a bridge to transfer the electron from the iron surface to the hydrogen ion.

The poisoning model of Bockris et al ¹⁰⁾ attributes the increase in hydrogen absorption to a lowering of the M-H_{ads} bond energy, w . Lowering of w increases the activation energy for the discharge process of the h.e.r. Thus, in systems where this model is applicable, the hydrogen overvoltage would increase with increasing concentration of the poison. However, it is now well established that H_2S decreases the hydrogen overpotential ^(3,4,5,8) and, thus, the poisoning model is not applicable in this case.

Bolmer ⁽¹¹⁾ proposed an overall reaction model:



and rationalized that at currents below the diffusion limited current, the hydrogen evolution mechanism is a function of the HS^- concentration and/or the $\text{H}_2\text{S}/\text{HS}^-$ ratio. However, his analysis was incomplete in that the reaction parameters for the h.e.r. and hydrogen absorption remained unknown.

In the studies cited above, the experimental data were not sufficient and the interpretations were based mostly on experiments which were not well defined. Also, up to the present time and because of its complexity there seems to be no general model which can rationalize the significant effect of H_2S on the h.e.r.

This paper reports the results of experimental studies directed at evaluating the effect of H_2S on the hydrogen permeation and evolution reactions. It analyzes these results with a newly developed general model of hydrogen entry into metals ^(12,13) in order to gain an insight into the permeation mechanism and to arrive at otherwise difficult-to-obtain parameters such as the surface coverage and the individual rate constants.

EXPERIMENTAL

A Devanathan-Stachurski cell (14) was used to measure the permeability of hydrogen through iron membranes as a function of the charging current, pH and H₂S concentration in the charging solution. The apparatus shown in Figure 2 consists of two identical electrolytic cells separated by the iron membrane. One of the membrane surfaces (input surface) was galvanostatically charged with hydrogen, using a Pt counter electrode. The potential of the input surface was measured with a saturated calomel reference electrode. The other membrane surface (exit surface) was coated with Pd and held in 0.1M NaOH at a potential of 150 mV (versus a HgO/Hg reference electrode) which oxidized all of the hydrogen diffusing through the membrane; this oxidation current provided a measure of the hydrogen permeation flux.

The membrane was Ferrovac E-Iron, annealed in evacuated capsules at 930°C for two hours and furnace cooled. The final preparation involved polishing with 600 emery paper and degreasing with a mixture of benzene and acetone. The final thickness of the iron specimen was 0.5mm and this iron membrane was fixed between the two cells, tightly sealing them with rubber O-rings. Details of the cell design, circuitry, edge effects, and special procedures can be seen elsewhere (15).

Mixtures of 0.1M HClO₄ and 0.1M NaClO₄ were used to make up the charging solutions with pH values of 1 and 2. The solutions were pre-electrolyzed for 72 hours under an atmosphere of prepurified nitrogen. To make up solutions containing H₂S, first a master solution of H₂S was prepared by passing H₂S gas of 99.6% purity through the deaerated, pre-electrolyzed 0.1M HClO₄ solution. The concentration of H₂S in this master solution was measured with an ion selective electrode and found to reach 5.2×10^{-2} M, after two hours of H₂S flow through the solution. The master solution of H₂S was mixed with the charging solution in order to give H₂S concentrations of 10^{-5} to 10^{-3} M, while maintaining the ionic strength constant.

In order to obtain reproducibility of the permeation data, several different precharging procedures were evaluated. The procedure that gave good reproducibility consisted of the following steps. The charging solution was pre-electrolyzed in a pre-electrolysis cell with Pt electrodes at 2 mA for more

than 72 hours prior to starting the experiment. Then, the iron membrane was precharged at 1 mA for 30 minutes and then at 0.5 mA for 3 hours (during this time, the charging potential moved in the negative direction as the permeation current increased). Following this step, the cell was drained and filled again with fresh pre-electrolyzed solution. Subsequently, the polarization and permeation data were recorded proceeding from a starting higher current ($\cong 1 \text{ mA cm}^{-2}$) to lower currents. To perform experiments with H_2S , the charging solution was changed to the H_2S pre-mixed solution and the same sequence was repeated.

RESULTS

The cathodic polarization curves for different H_2S concentrations ($c_{\text{H}_2\text{S}}$) in the charging solution at two different (acidic) pH values are given in Figures 3 (a) and (b). It is easily observed from these plots that the hydrogen overvoltage (η) decreases asymptotically with increasing H_2S concentration. Figures 4 (a) and (b) display the steady state permeation current (i_{∞}) as a function of the hydrogen overvoltage (η), for the pH1 and pH2 charging solutions. From these figures, it is obvious that i_{∞} increases substantially in the presence of H_2S . They also show that while all of the $\ln i_c$ vs η and $\ln i_{\infty}$ vs η plots in the non H_2S -containing solutions are linear, not all are linear in the presence of H_2S .

In order to understand the mechanism and quantitatively analyze the partitioning between the hydrogen absorption and hydrogen evolution reactions, the recently developed I-P-Z model (13) is applied here. According to this model, the i_{∞} vs $\sqrt{i_r}$ plot (where $i_r = i_c - i_{\infty}$ is the hydrogen recombination current density) and $f_{i\eta} (= i_c e^{a\alpha\eta})$ vs i_{∞} plot (where α is the h.e.r. transfer coefficient and $a = F/RT = 38.94 \text{ V}^{-1}$) will be linear if the mechanism of the h.e.r. is a non-activated (i.e., the energy of adsorption is not coverage dependent) discharge-chemical recombination process. Figure 5(a) shows that the relationship between i_{∞} and $\sqrt{i_r}$ is linear at pH=1, for solutions with and without H_2S . Figure 5(b) shows that the i_{∞} vs $\sqrt{i_r}$ plot is linear at pH=2 in the absence of H_2S and also when $c_{\text{H}_2\text{S}} = 2.5 \times 10^{-5} \text{ M}$ whereas it is nonlinear for the higher H_2S concentrations. The corresponding $f_{i\eta}$ vs i_{∞} plots are given in Figures 6 (a) & (b). Although there is a fair amount of scatter in Figure 6(a), mainly due to the lack of knowledge of the exact α values, the $f_{i\eta}$ vs. i_{∞} plot is found to be linear

for the lower H₂S containing pH1 solutions. On the other hand, for the pH2 solutions (Figure 6(b)), the $f_{i\eta}$ vs. i_{∞} plot is found to be linear for $c_{H_2S}=0$, but nonlinear for $c_{H_2S}=2.5 \times 10^{-5}$ M. Thus, for the higher pH and higher H₂S containing solutions, deviations occur in the square-root relationship (Figure 5(b)) or the $f_{i\eta}$ - i_{∞} plot becomes nonlinear (Figure 6(b)), or both.

ANALYSIS AND DISCUSSION

1. Data Analysis Using the Basic I-P-Z Model

Since the i_{∞} vs $\sqrt{i_r}$ and $f_{i\eta}$ vs i_{∞} plots are linear for the pH1 solutions except at the highest H₂S concentration, including $c_{H_2S}=0$ (Figures 5 (a) and 6 (a)) as well as for the pH2 solution at $c_{H_2S} = 0$ (Figures 5 (b) and 6 (b)), the basic I-P-Z model (13) can be applied for these cases. The following equations represent the fluxes or currents of the discharge, recombination and permeation reactions (symbols are defined at the end of the text) (13):

$$i_c = Fk_1 (1-\theta_H)e^{-\alpha\alpha\eta} = i_o' (1-\theta_H) e^{-\alpha\alpha\eta} \quad (1)$$

where $i_o' = F k_1^0 \theta_H + e^{-\alpha\alpha E^{c\eta}}$

$$i_r = F k_3 \theta_H^2 \quad (2)$$

$$i_{\infty} = F (D_1/L) c_s = c_s/b \quad (3)$$

$$\theta_H = c_s/k'' \quad (3a)$$

$$k'' = k_{abs}/(k_{ads} + (D_1/L)) \quad (3b)$$

And from these equations, the following relationships have been obtained(13):

$$i_{\infty} = (k''/b) (F k_3)^{-0.5} \sqrt{i_r} \quad (4)$$

$$i_c e^{\alpha\alpha\eta} = - (b i_o' / k'') i_{\infty} + i_o' \quad (5)$$

Thus, from Figures 5 and 6 (in essence, by regression analysis of Equations (4) and (5)) and Eq. (1), all of the following constants are computed: the exchange current density, $i_o (=i_o' (1-\theta_c))$; the discharge reaction rate constant, k_1^0 ; the recombination reaction rate constant, k_3 , and the thickness dependent absorption-adsorption constant, k'' . For details of the computation procedure, see elsewhere (13).

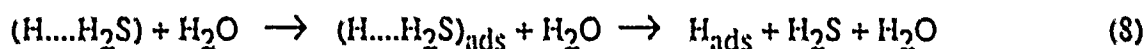
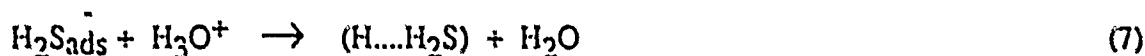
2. Modified I-P-Z Model Incorporating Frumkin-Temkin Correction for Activated Reactions

For pH = 2, the presence of H₂S causes a deviation from a linear $i_{ca} \propto \sqrt{i_r}$ behavior (Figure 5(b)) or linear $f_{i\eta} \propto i_{ca}$ behavior (Figure 6(b)). One possibility is the adsorption of HS⁻ but this would require that the pH in the interface region rise above -4.5 since it is clear from Figure 1 that the dissociation of H₂S is negligible in solutions of pH ≤ 4.5. Another is that H₂S⁻ can be formed (16,17) by the following reaction:



having a high reaction rate constant. This fast side reaction occurring at the cathodic metal surface can have three different effects:

(1) H₂S can function as a bridge for hydrogen discharge through the H₂S⁻ species, similar to the proposal by Kawashima et al (3):



where H₂S⁻_{ads} discharges the proton (Eq. (7)) and becomes the stable H₂S molecule (Eq. (8)). This step can decrease the overvoltage for the discharge reaction, in accord with the experimental observations (Figures 3 (a) and (b)).

(2) Besides the above effect, the recombination reaction can also be restricted effectively by the (H...H₂S) intermediate of this side reaction slowing the diffusion of hydrogen adatoms and/or blocking the hydrogen recombination sites on the metallic surface.

(3) At higher pH, in view of the higher [H₂S]/[H⁺] ratio, chemical desorption is less strongly favored; i.e., effect 2 could lead to a change in the mechanism from a primarily chemical desorption to an electrochemical desorption mechanism.

The adsorption of HS⁻ on the surface can produce the same result as the (H...H₂S) species in effects (2) and (3) but HS⁻ cannot match H₂S⁻ in facilitating the proton discharge step (effect (1)) because HS⁻, unlike H₂S, is not stable so the bridge mechanism is the more likely one. The above effects (2) and (3) indicate activation of the hydrogen evolution reaction (h.e.r.) and under these

conditions, the Frumkin-Temkin (F-T) corrections have to be applied to the discharge and recombination currents (18); thus, Equations (1) and (2) will be modified as follows:

$$i_c = i_o' (1-\theta_H) e^{-\alpha a \eta} e^{-\alpha f \theta_H} \quad (9)$$

$$i_r = F k_3 \theta_H^2 e^{2\alpha f \theta_H} \quad (10)$$

where $f = \gamma/RT$ and γ is the gradient of the apparent standard free energy of adsorption with coverage. Although not considered in Eqs. (8) and (9), the coverage by H_2S^* may also be important as far as site availability and activation of the reactions are concerned. In order to determine the effect of H_2S , the relationship between θ_H and $\theta_{H_2S^*}$ needs to be quantified by considering the change in θ_H by additions of H_2S to the solution. The implicit assumption in the present model is that this H_2S effect can be neglected as if the H_2S^* , in acting as a bridge to discharge the proton, will not occupy a surface site for a prolonged duration. A typical value of f is 4 to 5 for hydrogen coverages (18); $f = 4.5$ will be used here.

From Equations (3) and (3a) we obtain,

$$\theta_H = b i_{\infty} / k'' \quad (11)$$

Inserting Equation (11) into Equation (10), it can be shown that

$$\ln (\sqrt{i_r/i_{\infty}}) = (\alpha f b / k'') i_{\infty} + \ln \{ b (F k_3)^{0.5} / k'' \} \quad (12)$$

Substituting θ_H from Equation (11) into Equation (9), one obtains

$$\ln [i_c e^{(\alpha f b i_{\infty} / k'') / (1 - b i_{\infty} / k'')}] = -\alpha a \eta + \ln (i_o') \quad (13)$$

or

$$\ln (f_{i_c, i_{\infty}}) = -\alpha a \eta + \ln (i_o') \quad (14)$$

where

$$f_{i_c, i_{\infty}} = i_c e^{(\alpha f b i_{\infty} / k'') / (1 - b i_{\infty} / k'')} \quad (14a)$$

Thus, Equation (12) tells us that i_{∞} will not be linearly related to $\sqrt{i_r}$, when the h.e.r. is activated ($f > 0$), but that i_{∞} will be linearly related to $\ln (\sqrt{i_r/i_{\infty}})$. Also, according to Equation (14), $\ln (f_{i_c, i_{\infty}})$ will be linearly related to η when the h.e.r. is activated.

3. Data Analysis by the Application of F-T Corrected I-P-Z Model

Figure 7 shows that the plots of $\ln(\sqrt{i_r}/i_{\infty})$ vs i_{∞} at pH = 2 are linear in accord with Equation (12) for $c_{\text{H}_2\text{S}}=10^{-4}$ M and $c_{\text{H}_2\text{S}}=3 \times 10^{-4}$ M. But for the lowest H_2S concentration, $c_{\text{H}_2\text{S}}=2.5 \times 10^{-5}$ M, the plot may not be completely linear and is consistent with the h.e.r. being only partially activated, as is already indicated above in the i_{∞} vs $\sqrt{i_r}$ plot (Figure 5(b)) which is linear and in the $f_{i\eta}$ vs i_{∞} plot (Figure 6(b)) which is nonlinear. Extended analysis showed that the data for $c_{\text{H}_2\text{S}}=2.5 \times 10^{-5}$ M are better analyzed with the F-T corrected I-P-Z model.

The value of α is determined from Equations (12) and (14) by an iterative procedure. Using an initial value of $\alpha = 0.5$ and the k'' obtained from the slope of the $(\sqrt{i_r}/i_{\infty})$ vs. i_{∞} plot (Eq. (12)), $\ln(f_{i_c, i_{\infty}})$ is known for various values of i_c and i_{∞} and as a function of η . Thus, a regression analysis of Eq. (14) can be done to obtain a new value of α . Using this new value of α , a new value of k'' is obtained (from Eq. (12)) and a regression analysis is again performed on Eq. (14). This procedure is repeated until the α obtained from the slope of the $\ln(f_{i_c, i_{\infty}})$ vs η plot (Eq. (14)) converges to a fixed value. Then, the $\ln(f_{i_c, i_{\infty}})$ vs η functions are plotted (Figure 8), and, besides α , k_3 , k'' and i_0' are determined from the regression analysis of Equations (12) and (14).

Having determined k'' for all combinations of pH and $c_{\text{H}_2\text{S}}$ (ie. with and without the F-T correction to the I-P-Z model), θ_{H} (calculated using Equation (11)) vs η can be plotted and these are shown in Figures 9 (a) and (b). These plots demonstrate that H_2S increases the hydrogen surface coverage (θ_{H}) quite significantly and that the increase is asymptotic with increasing $c_{\text{H}_2\text{S}}$. In fact, at pH = 2 (Figure 9 (b)), the θ_{H} values increase significantly with small additions of H_2S , but do not increase any further with higher $c_{\text{H}_2\text{S}}$ within the experimental error. One explanation of this asymptotic behavior is that the adsorption sites, which could be a small fraction of the total surface sites, e.g., kinks, become occupied at low H_2S concentrations. Thus, the effectiveness of H_2S in slowing down the diffusion of H atoms on the surface and/or blocking the recombination sites with side reaction (6), thereby increasing θ_{H} , reaches a saturation limit. Another explanation is that H_2S adsorbs readily on the surface and at rather low H_2S concentrations in the solution begins to interfere with adsorption sites for hydrogen on the surface. The limit of this effect could be a decrease in θ_{H} with increasing H_2S concentration, which is not observed in Figs. 8 and 9. The equilibrium hydrogen

Figure 7 shows that the plots of $\ln(\sqrt{i_r/i_{\infty}})$ vs i_{∞} at pH = 2 are linear in accord with Equation (12) for $c_{H_2S} = 10^{-4}$ M and $c_{H_2S} = 3 \times 10^{-4}$ M. But for the lowest H_2S concentration, $c_{H_2S} = 2.5 \times 10^{-5}$ M, the plot may not be completely linear and is consistent with the h.c.r. being only partially activated, as is already indicated above in the i_{∞} vs $\sqrt{i_r}$ plot (Figure 5(b)) which is linear and in the $f_{i\eta}$ vs i_{∞} plot (Figure 6(b)) which is nonlinear. Extended analysis showed that the data for $c_{H_2S} = 2.5 \times 10^{-5}$ M are better analyzed with the F-T corrected I-P-Z model.

The value of α is determined from Equations (12) and (14) by an iterative procedure. Using an initial value of $\alpha = 0.5$ and the k'' obtained from the slope of the $(\sqrt{i_r}/i_{\infty})$ vs. i_{∞} plot (Eq. (12)), $\ln(f_{i_c, i_{\infty}})$ is known for various values of i_c and i_{∞} and as a function of η . Thus, a regression analysis of Eq. (14) can be done to obtain a new value of α . Using this new value of α , a new value of k'' is obtained (from Eq. (12)) and a regression analysis is again performed on Eq. (14). This procedure is repeated until the α obtained from the slope of the $\ln(f_{i_c, i_{\infty}})$ vs η plot (Eq. (14)) converges to a fixed value. Then, the $\ln(f_{i_c, i_{\infty}})$ vs η functions are plotted (Figure 8), and, besides α , k_3 , k'' and i_0' are determined from the regression analysis of Equations (12) and (14).

Having determined k'' for all combinations of pH and c_{H_2S} (ie. with and without the F-T correction to the I-P-Z model), θ_H (calculated using Equation (11)) vs η can be plotted and these are shown in Figures 9 (a) and (b). These plots demonstrate that H_2S increases the hydrogen surface coverage (θ_H) quite significantly and that the increase is asymptotic with increasing c_{H_2S} . In fact, at pH = 2 (Figure 9 (b)), the θ_H values increase significantly with small additions of H_2S , but do not increase any further with higher c_{H_2S} within the experimental error. One explanation of this asymptotic behavior is that the adsorption sites, which could be a small fraction of the total surface sites, e.g., kinks, become occupied at low H_2S concentrations. Thus, the effectiveness of H_2S in slowing down the diffusion of H atoms on the surface and/or blocking the recombination sites with side reaction (6), thereby increasing θ_H , reaches a saturation limit. Another explanation is that H_2S adsorbs readily on the surface and at rather low H_2S concentrations in the solution begins to interfere with adsorption sites for hydrogen on the surface. The limit of this effect could be a decrease in θ_H with increasing H_2S concentration, which is not observed in Figs. 8 and 9. The equilibrium hydrogen

coverage (θ_e) can be obtained by extrapolating the θ_H vs η plots to $\eta = 0$, and these plots are in Figure 9c. Then, i_0 is obtained as: $i_0 = i_0' (1 - \theta_e)$, and k_1^0 is obtained from Eq. 1.

4. H_2S Effects on the Various Kinetic Parameters and the h.e.r. Transfer Coefficient

In order to thoroughly and quantitatively understand the mechanism by which H_2S enhances hydrogen entry into iron, all of the important quantities are plotted versus c_{H_2S} (Figures 10 to 15). Figure 10 shows a plot of i_0 as a function of c_{H_2S} , indicating that i_0 is unaffected by H_2S . On the other hand, α is increased significantly by small additions of H_2S as shown in Figure 11. Figure 11 also shows within the experimental scatter that α asymptotically reaches a concentration independent value at higher concentrations of H_2S . The general increase in α can be explained by the Kawashima, et. al., bridge mechanism (described earlier) that facilitates easier proton discharge, and the asymptotic behavior of α with c_{H_2S} may be a consequence of the H_2S^- saturation discussed above.

A plot of the discharge rate constant (k_1^0) as a function of c_{H_2S} , Figure 12, shows that k_1^0 is unaffected by H_2S . The large scatter in Figure 12 may be due to the actual desorption mechanism being partly chemical recombination and partly electrochemical, especially when the c_{H_2S} is high since, as is reported below, chemical recombination less readily occurs with increasing H_2S concentration. Due to the extreme complexity of this problem and a lack of the pertinent kinetic data, an analysis considering both of these desorption mechanisms simultaneously is not being pursued at present.

Another important parameter is the thickness dependent absorption-adsorption constant (k'') plotted as a function of c_{H_2S} (Figure 13), showing that k'' is not altered significantly by H_2S . The slight increase that may be indicated in Figure 13 means that absorption is favored over adsorption with increasing H_2S concentration. Hence along with the increasing α and decreasing k_3 (reported below), an increasing k'' may also contribute to the increase in steady state permeation with increasing H_2S concentration. An increase in k'' could be caused by any of the factors associated with the energy of adsorption becoming coverage dependent. The data in Figure 13 include those for $pH = 1$ (without F-T-c) and also those for $pH = 2$ (with F-T-c) and they seem to merge quite well, further supporting the proposed mechanism.

From the foregoing discussion, the H₂S bridging during hydrogen discharge (reactions (7) & (8)) and the activation of the h.e.r. by H₂S (i.e. the slowing down of the diffusion of hydrogen atoms and/or the blocking of the hydrogen recombination sites) are considered to be the two major effects of H₂S. A further confirmation of the importance of these effects of H₂S would be a significant decrease in the recombination rate constant with increasing $c_{\text{H}_2\text{S}}$. Indeed, that this occurs, is clear from Figure 14, which shows k_3 decreases with addition of H₂S to the solution and as with the other parameters, then levels off with further additions of H₂S.

5. Hydrogen Evolution Reaction Mechanism

Finally, the potential range in which the coupled discharge-recombination mechanism operates can also be determined from the I-P-Z model (13) as follows:

$$\eta_c^l = [\ln (10 k_1/k_3)]/(\alpha\alpha) \quad (15)$$

$$\eta_c^u = [\ln (0.1 k_1/k_3)]/(\alpha\alpha) \quad (16)$$

where η_c^l is the lower limit and η_c^u is the upper limit of the potential range. The calculated values of η_c^l and η_c^u are plotted in Figure 15, as a function of $c_{\text{H}_2\text{S}}$ and c_{H^+} . The two solid slanted lines are drawn, one through the lower points and one through the upper points, to indicate the lower and upper bounds of the hydrogen overvoltages calculated for the coupled discharge-recombination mechanism using the k_1 , k_3 and α values obtained by application of the model to the data for the different H₂S concentrations, while the horizontal lines at $\eta = -0.35$ and $\eta = -0.45$ V indicate the lower and upper bounds of the experimentally measured hydrogen overvoltages. For example, in the absence of H₂S (which corresponds to the abscissa value of zero), the experimental overvoltage range is at less negative electrode potentials than the overvoltage range for operation of the coupled discharge-recombination mechanism. So, the discharge reaction may be rate controlling in this case. But with increasing $c_{\text{H}_2\text{S}}$, the overpotential range for operation of the coupled discharge-recombination mechanism shifts to lower overpotentials so that above a certain combination of the concentrations of H₂S and H⁺ (i.e., $[\text{H}_2\text{S}]^{0.25}/[\text{H}^+]^{0.125} \gtrsim 0.2$), this range overlaps the overpotential range of the experiments (shaded region in Figure 15). Thus, with increasing H₂S concentration, the h.e.r. mechanism shifts from proton discharge controlled to coupled discharge-recombination controlled.

At higher pH values, one would expect that the effect of H_2S in slowing the diffusion of hydrogen atoms will be even larger because of the higher $[H_2S]/[H^+]$ ratio. What this would mean is that the mechanism of H_2 formation (i.e. hydrogen recombination) may have to change into an electrochemical desorption mechanism at higher pH values. This prediction is fully consistent with the findings of Murayama et al (19) in that the electrochemical combination route (i.e. $H_{ads} + H^+ + e^- \rightarrow H_2$) dominates over the chemical combination route for 99.9% iron in acetate solutions of $pH > 3$ in the presence of H_2S .

One final comment is to be made with regard to the importance of the Equation (3b) in enlightening our understanding of the surface and near surface reaction kinetics. Rewriting Equation (3b), we obtain

$$(k'')^{-1} = (k_{ads}/k_{abs}) + (D_1/k_{abs})(L)^{-1} \quad (17)$$

Equation (17) has been discussed elsewhere⁽¹³⁾. The essence of Equation (17) is that if the plot of $1/k''$ vs $1/L$ is linear, the values of k_{abs} and k_{ads} are obtained (knowing D_1). Thus, from the complete polarization and permeation data for different membrane thicknesses (L), one can systematically investigate the important surface properties relating to the hydrogen absorption and adsorption rate constants.

CONCLUSIONS

1. Cathodic hydrogen charging experiments were performed on Ferrovac E-Iron membranes in perchloric acid solutions of pH 1 and 2 with and without H_2S . The steady-state, hydrogen permeation current density (i_∞) was greatly enhanced in the presence of H_2S , while the hydrogen overvoltage (η) was decreased.

2. The recently developed I-P-Z model (13) is applicable to the h.e.r./hydrogen permeation process in the absence of H_2S and for the pH 1 solutions of lower H_2S concentrations. From the analysis the various rate constants, exchange current density, transfer coefficient and hydrogen surface coverage were obtained.

3. For the higher pH and higher H₂S concentrations, the I-P-Z model was modified by utilizing the Frumkin-Temkin correction for the proton discharge and hydrogen recombination reactions. This correction was necessary due to the energy of adsorption becoming coverage dependent, probably a result of the product of the fast side reaction, $\text{H}_2\text{S} + \text{e}^- \rightarrow \text{H}_2\text{S}^-_{\text{ak}}$, restricting the diffusion of hydrogen adatoms and/or blocking the hydrogen recombination sites on the iron surface.

4. The hydrogen surface coverage (θ_{H}) and the transfer coefficient (α) are enhanced while the recombination rate constant (k_3) is decreased in the presence of H₂S. The increase in α explains the observed decrease in overpotential (η) on the basis of the Kawashima et al (3) bridging effect of H₂S⁻ (i.e., the overall reaction: $\text{H}_2\text{S}^-_{\text{ak}} + \text{H}_3\text{O}^+ \rightarrow \text{H}_{\text{ads}} + \text{H}_2\text{S} + \text{H}_2\text{O}$).

5. On the basis of the bridging effect and the slowing of the recombination reaction, all of the observations and calculated parametric changes by H₂S have been rationally explained. These parametric changes are the increase in the transfer coefficient (α) and the decrease in the recombination reaction rate constant (k_3). In addition, the overvoltage range for operation of the coupled discharge-recombination mechanism is predicted, by application of the I-P-Z model to the data, to be at lower overpotentials in the presence of H₂S and to overlap the experimentally measured overpotentials above a certain H₂S concentration, i.e., the h.e.r. mechanism shifts from discharge controlled to coupled discharge-recombination controlled with increasing H₂S concentration.

6. It is noteworthy that one can now calculate the important hydrogen absorption and adsorption rate constants, by applying the I-P-Z model to the electrochemical permeation data obtained as a function of membrane thickness.

ACKNOWLEDGMENT

The encouragement and financial support by A. John Sedriks, Office of Naval Research, Contract No. N00014-84K-0201 are gratefully acknowledged.

LIST OF SYMBOLS

- a a constant, F/RT , (volts)⁻¹
 a_{H^+} activity of hydrogen ions in the electrolyte, dimensionless

A	amperes
b	a constant, L/FD_1 , mol (A cm)^{-1}
c_{H^+}	hydrogen ion concentration, $10^{-\text{pH}}$, mol liter^{-1}
$c_{\text{H}_2\text{S}}$	H_2S concentration in the electrolyte, mol liter^{-1}
c_s	surface hydrogen concentration, mol cm^{-3}
D_1	bulk hydrogen diffusion coefficient, $\text{cm}^2 \text{s}^{-1}$
E_{eq}	equilibrium potential for the h.c.r., mV vs SHE
F	Faraday constant, $96500 \text{ C g-eq}^{-1}$
f	a constant = γ/RT , dimensionless
f_{i_c, i_∞}	a variable, $i_c e^{(\alpha b i_\infty / k'') / (1 - b i_\infty / k'')}$, A cm^{-2}
f_{i_η}	a variable, $i_c e^{\alpha \eta}$, A cm^{-2}
i_c	charging flux or current density, A cm^{-2}
i_∞	steady state permeation flux, A cm^{-2}
i_0	exchange current density, A cm^{-2}
i_0'	$i_0 / (1 - \theta_c)$, A cm^{-2}
i_r	steady state evolution flux, A cm^{-2}
k_1^0	discharge reaction rate constant, $\text{mol (cm}^2 \text{s)}^{-1}$
k_1	discharge reaction rate coefficient (= i_0' / F), $\text{mol (cm}^2 \text{s)}^{-1}$
k_3	recombination reaction rate constant, $\text{mol (cm}^2 \text{s)}^{-1}$
k_{abs}	absorption rate constant, $\text{mol (cm}^2 \text{s)}^{-1}$
k_{ads}	adsorption rate constant, cm s^{-1}
k''	thickness dependent absorption-adsorption constant, mol cm^{-3}
L	membrane thickness, cm
M	mol liter^{-1}
R	gas constant, $8.314 \text{ J (g-mol K)}^{-1}$
T	temperature, K

Greek Symbols

α	transfer coefficient, dimensionless
η	overvoltage, V
η_c	cathodic overvoltage, V
η_c^l	lower limit of η_c , V
η_c^u	upper limit of η_c , V
θ_H	surface hydrogen coverage, dimensionless

- θ_c equilibrium surface hydrogen coverage, dimensionless
 γ gradient of the apparent standard free energy of adsorption with hydrogen coverage, J g-mol⁻¹

REFERENCES

1. H₂S Corrosion in Oil and Gas Production, A Compilation of Classic Papers, R. D. Tuttle and R. S. Kane, eds., NACE (1981).
2. J. F. Newman and L. L. Shreir, *Corrosion Science*, Vol. 9, p. 631 (1969).
3. A. Kawashima, K. Hashimoto and S. Shimodaira, *Corrosion*, Vol. 32, p. 321 (1976).
4. P. Sury, *Corrosion Science*, Vol. 16, p. 879 (1976).
5. M. Hashimoto, E. Sato and T. Murata, Hydrogen in Metals (Conf. Proc.), JIMS-2 (1980), p. 209
6. B. J. Berkowitz and H. H. Horowitz, *J. Electrochem. Soc.*, Vol. 129, p. 468 (1982).
7. J. O'M. Bockris, International Conference on Stress Corrosion Cracking and Hydrogen Embrittlement of Iron Base Alloys, Firminy, France, 1973, R. W. Staehle et al eds., NACE-5 (1977), p. 286.
8. Z. A. Iofa and F. L. Kam, *Zashchita Metallov*, Vol. 10, p. 17 (1974); *Protection of Metals*, Vol. 10, p. 12 (1974).
9. B. E. Boucher, Proceedings of the Fourth International Congress on Metallic Corrosion, NACE (1969), p. 550.
10. J. O'M. Bockris, J. McBreen and L. Nanis, *J. Electrochem. Soc.*, Vol. 112, p. 1025 (1965).
11. P. W. Bolmer, *Corrosion*, Vol. 21, p. 69 (1965).
12. R. N. Iyer, H. W. Pickering and M. Zamanzadeh, *Scripta Met.*, Vol. 22, p. 911 (1988).
13. R. N. Iyer, H. W. Pickering and M. Zamanzadeh, *J. Electrochem. Soc.*, 136, 7463 (1989).
14. M. A. Devanathan and L. Stachurski, *J. Electrochem. Soc.*, Vol. 111, p. 619 (1964).
15. S. S. Chatterjee, B. G. Ateya and H. W. Pickering, *Met. Trans.*, Vol. 9A, p. 389 (1978).
16. Private Discussions with Konrad Weil, Technische Hochschule Darmstadt, Darmstadt, Federal Republic of Germany.
17. E. Hart and M. Anbar, The Hydrated Electron, John Wiley & Sons, Inc., New York (1970), p. 113.
18. E. Gileadi and B. E. Conway, Modern Aspects of Electrochemistry, No. 3, J. O'M. Bockris and B. E. Conway, eds., Butterworths, Washington (1964), pp. 347-442.
19. H. Murayama, M. Sakashita and N. Sato, Hydrogen in Metals (Conf. Proc.), JIMS-2 (1980), p. 297.

FIGURE CAPTIONS

- Figure 1: Stability plots of H_2S , HS^- and S^{2-} as a function of pH. (9)
- Figure 2: Schematic of the apparatus for the hydrogen permeation experiment.
- Figure 3: Hydrogen overvoltage, η , vs. hydrogen charging current density i_c , for different H_2S concentrations at (a) pH=1 and (b) pH=2.
- Figure 4: Hydrogen overvoltage, η , vs. steady state hydrogen permeation current density, i_∞ , for different H_2S concentrations at (a) pH=1 and (b) pH=2.
- Figure 5: Steady state hydrogen permeation current density, i_∞ , vs. square root of hydrogen recombination current density, $\sqrt{i_r}$, for different H_2S concentrations at (a) pH=1 and (b) pH=2.
- Figure 6: Relationship between $f_{i\eta}$ and i_∞ for different H_2S concentrations at (a) pH=1 and (b) pH=2.
- Figure 7: Relationship between $\sqrt{i_r}/i_\infty$ and i_∞ for different H_2S concentrations at pH=2.
- Figure 8: Hydrogen coverage-corrected i_c vs hydrogen overvoltage, η , for different H_2S concentrations at pH=2.
- Figure 9: Hydrogen coverage, θ_{H} , vs hydrogen overvoltage, η , for different H_2S concentrations at (a) pH=1 and (b) pH=2.
- Figure 10: H_2S effect on the h.e.r. exchange current density, i_0 .
- Figure 11: H_2S effect on the h.e.r. transfer coefficient, α .
- Figure 12: H_2S effect on the discharge rate constant, k_1^0 .
- Figure 13: H_2S effect on the absorption-adsorption constant, k'' .
- Figure 14: H_2S effect on the hydrogen recombination reaction rate constant, k_3 .
- Figure 15: H_2S effect on the hydrogen overvoltage range (between sloped lines) of the coupled discharge-recombination mechanism. Points: Calculated

(Eqs. 15 and 16) for different k_1 and k_3 values obtained by application of the I-P-Z model to the permeation data. Cross hatched area: potential range of experimentation overlaps potential range of coupled discharge-recombination mechanism.

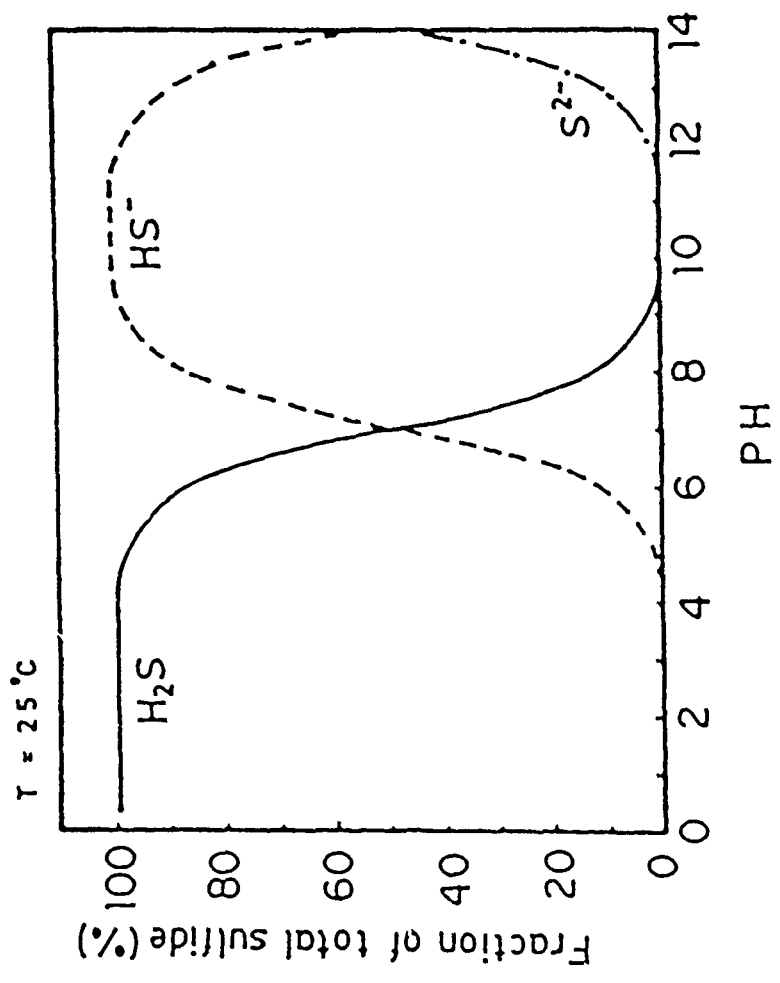


Fig. 1

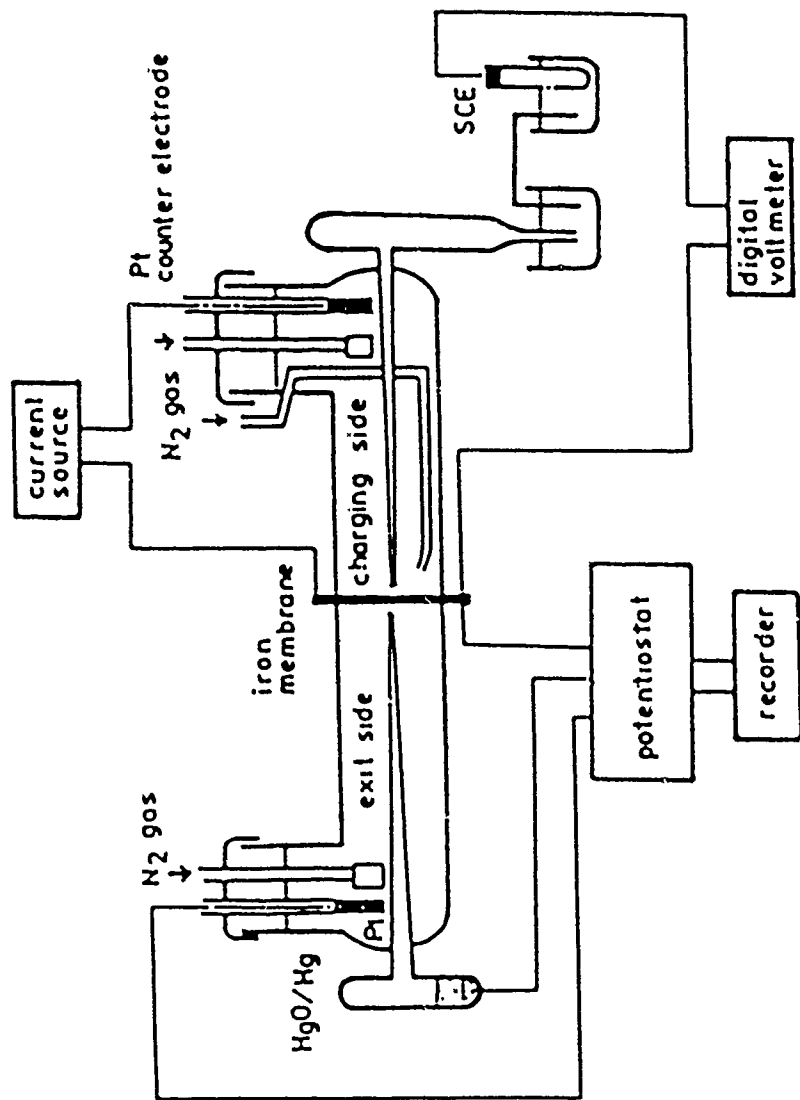


Fig. 2

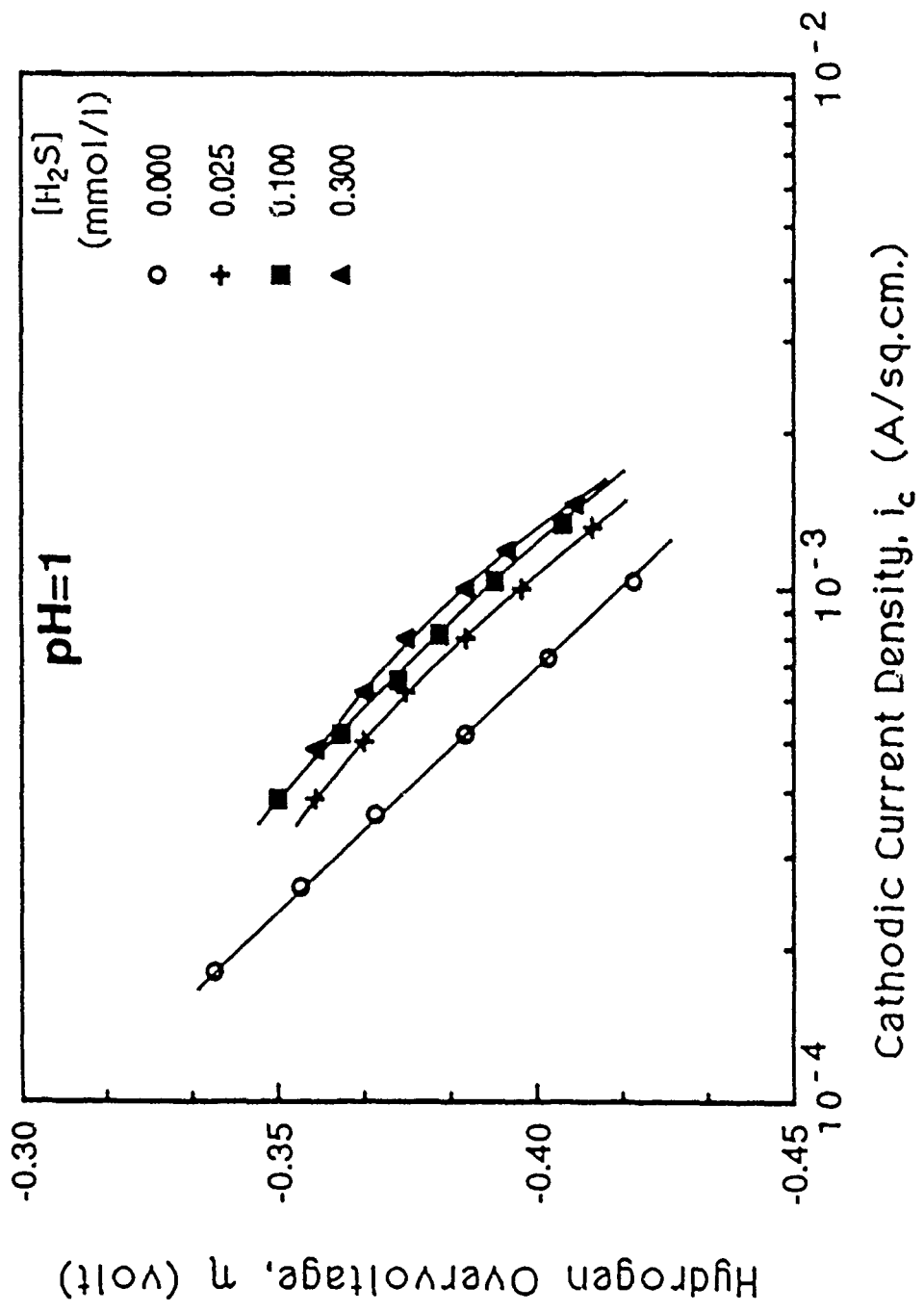


Fig. 3a

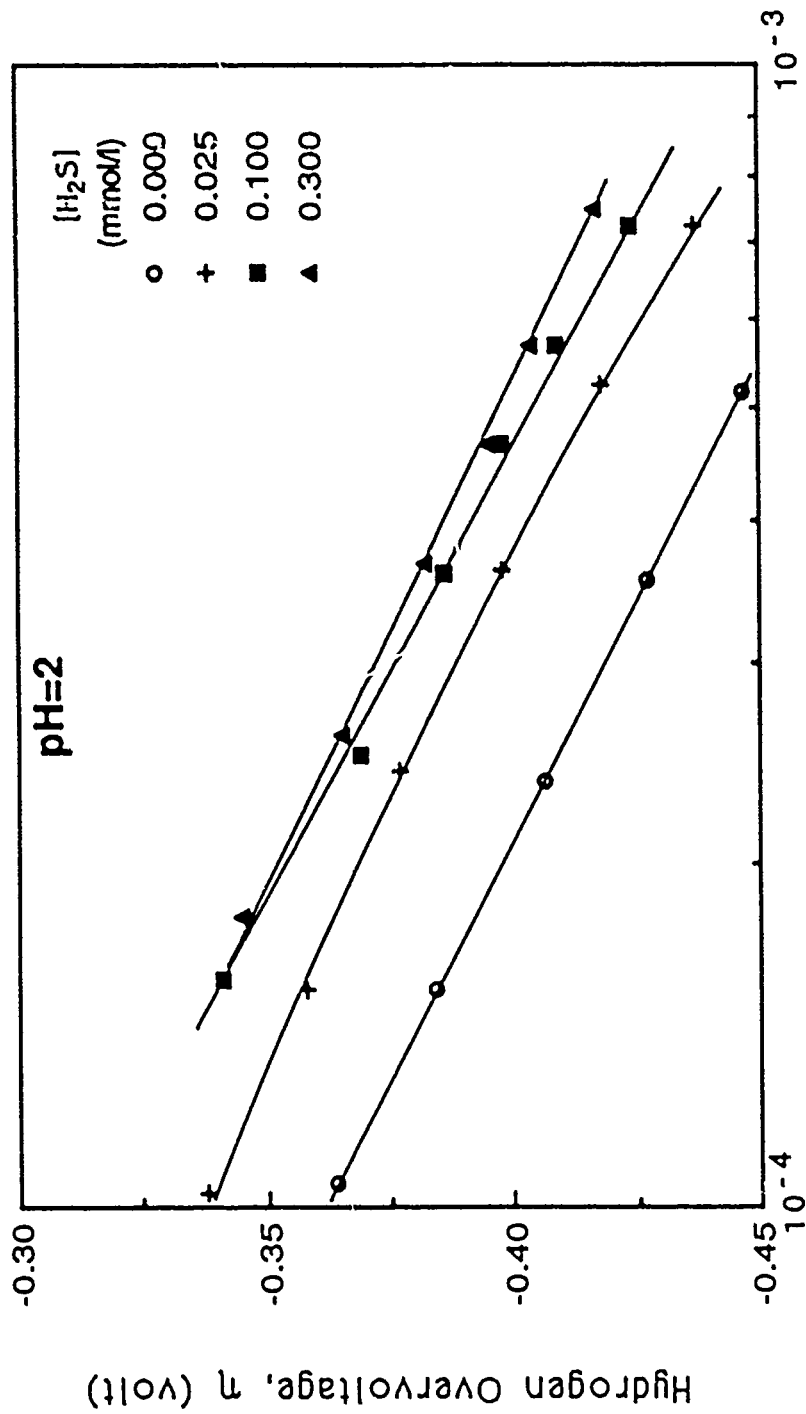


Fig. 3b

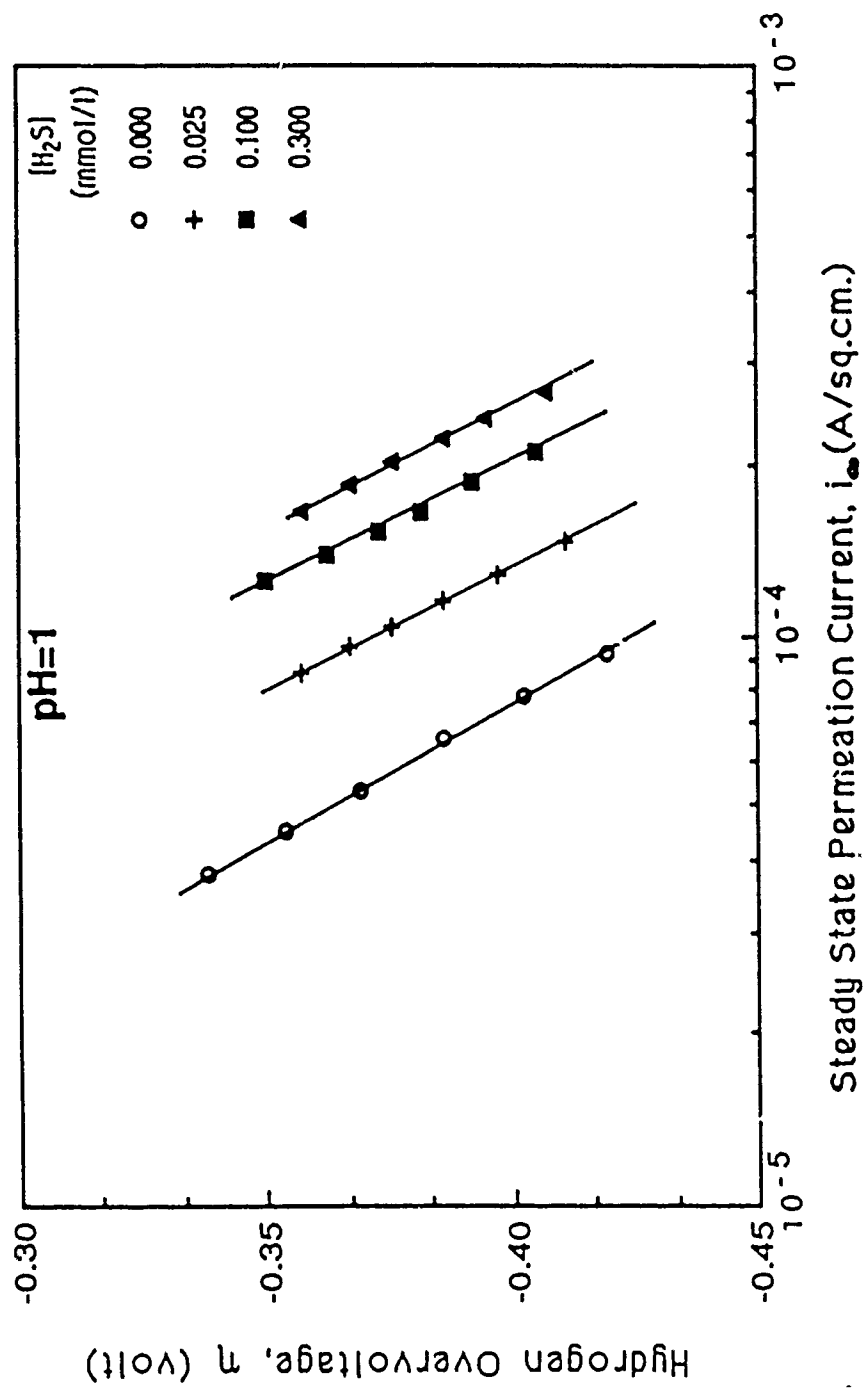


Fig. 4

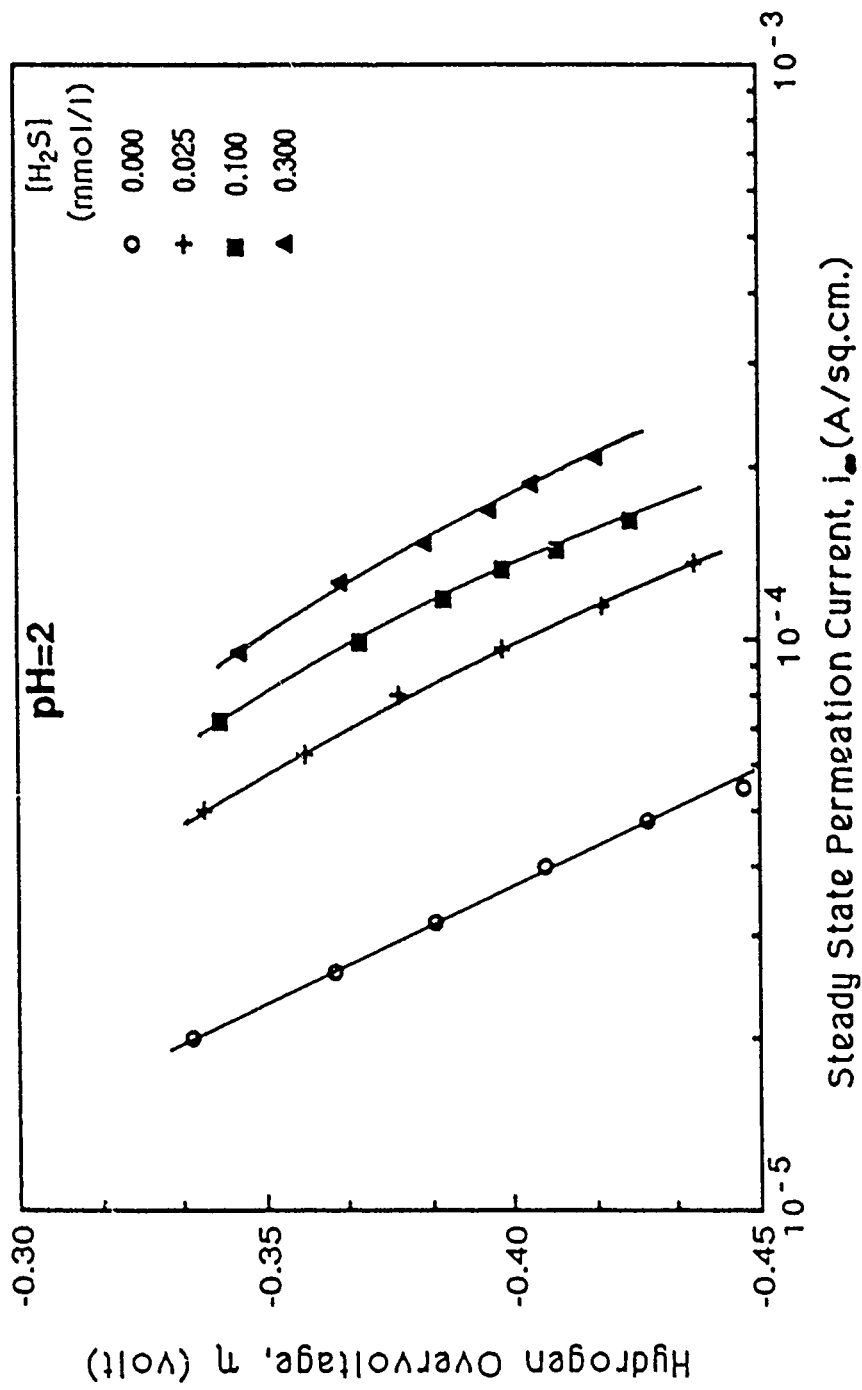


Fig. 4b

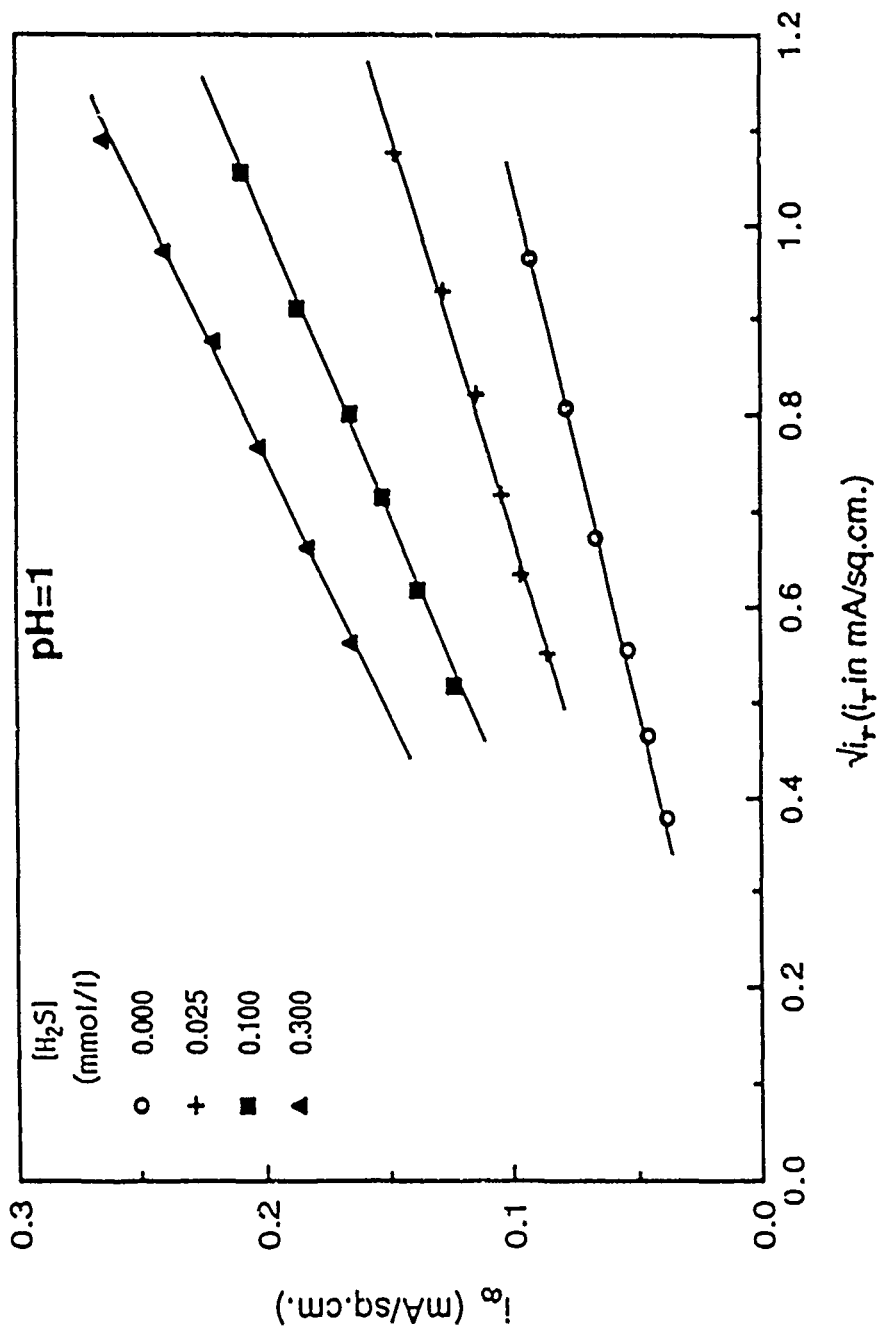


Fig. 5a

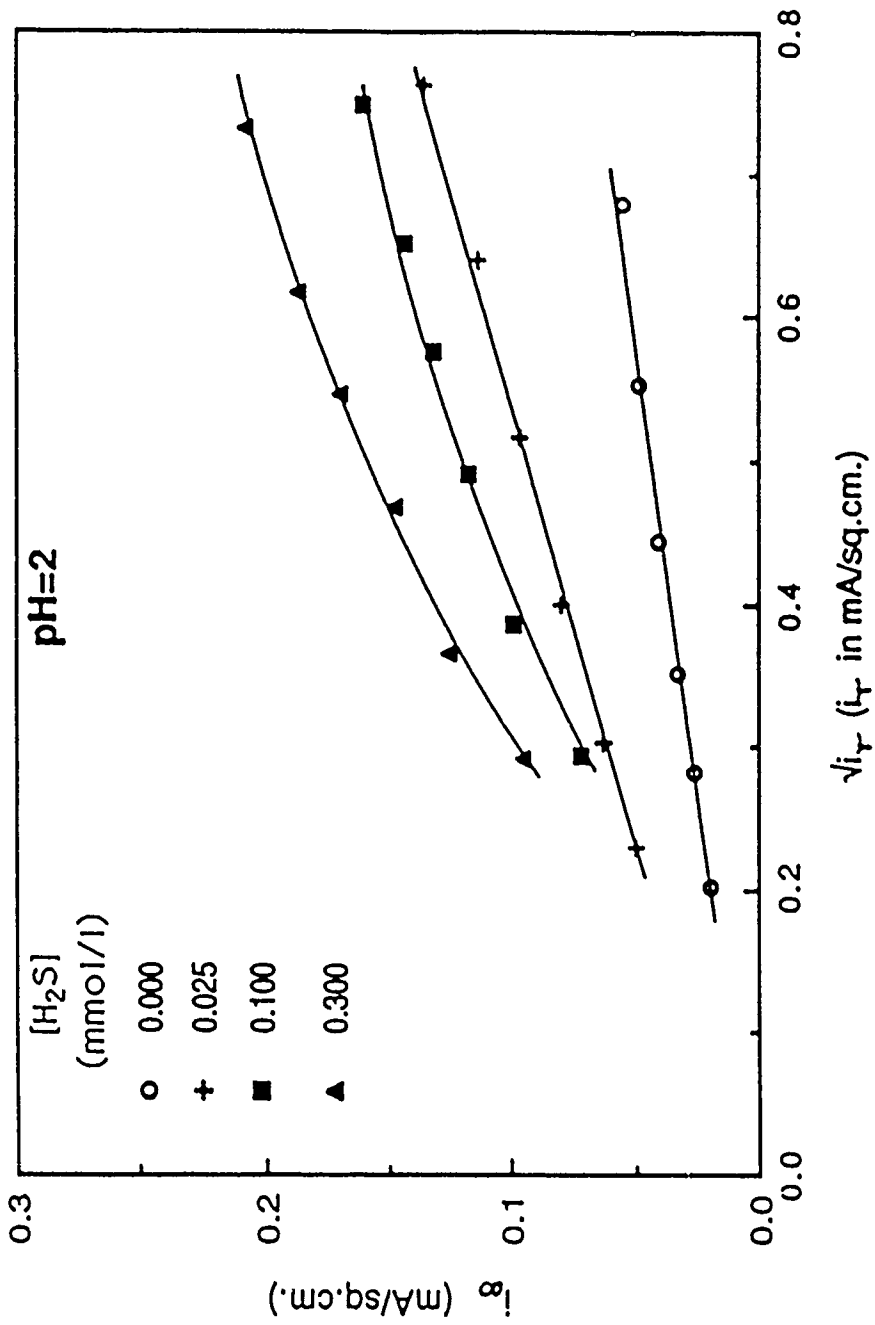


Fig. 5b

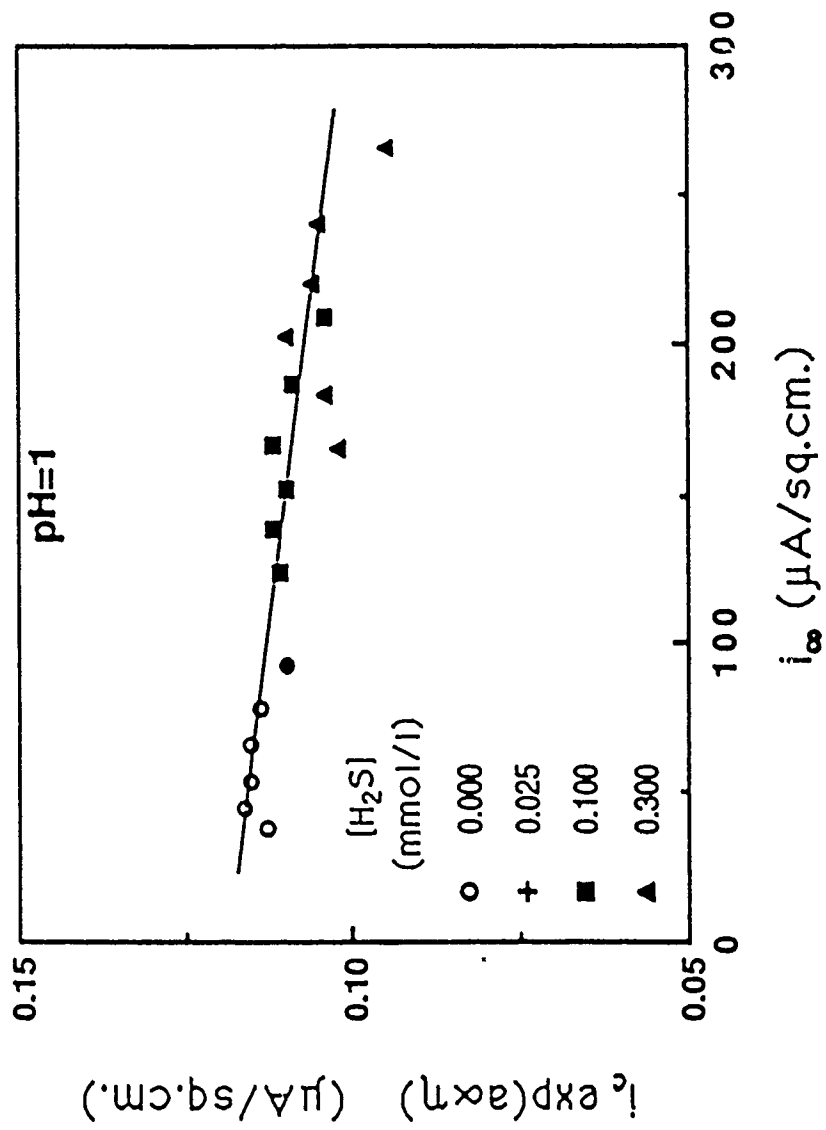


Fig. 6a

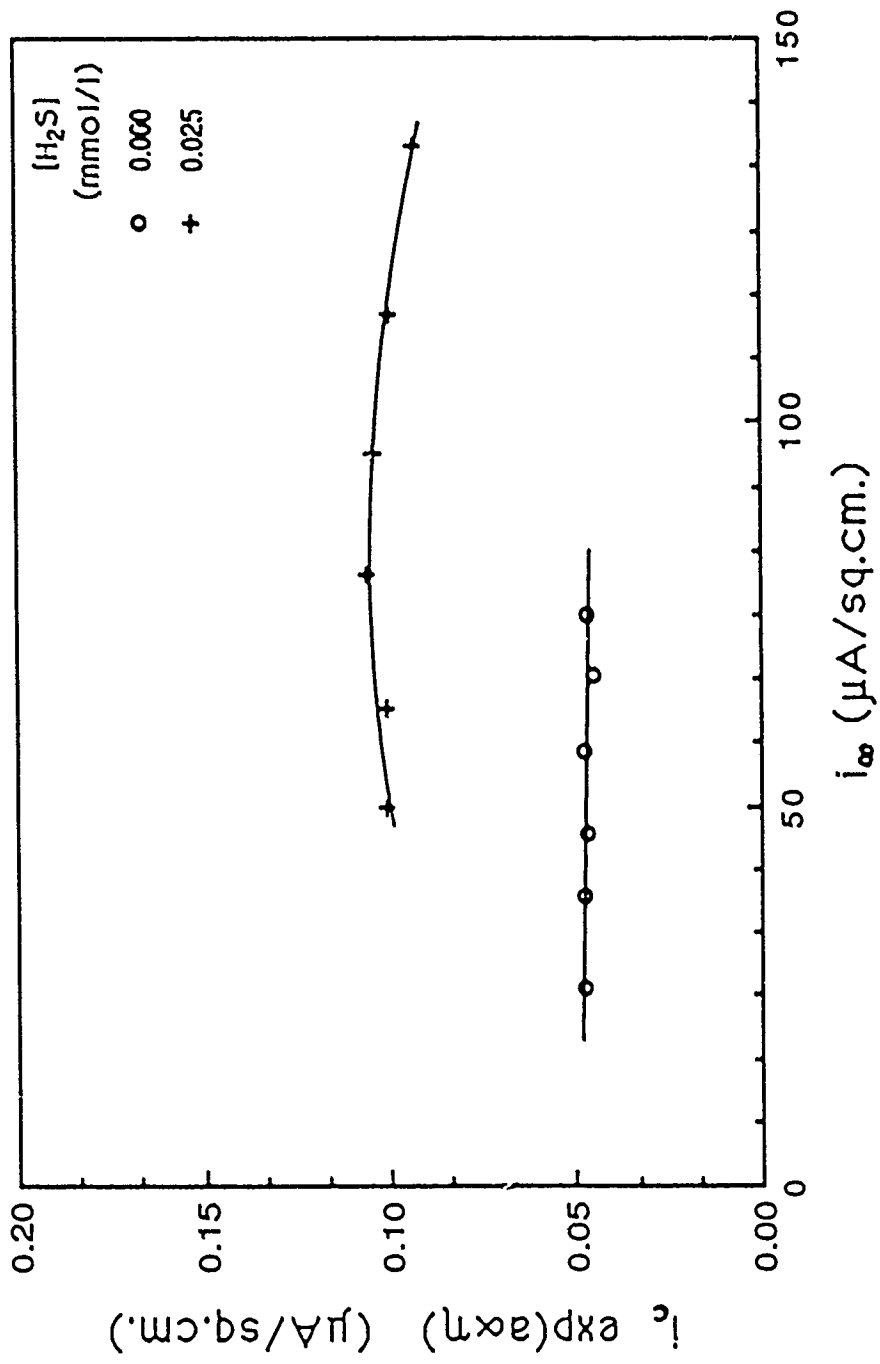


Fig. 6b

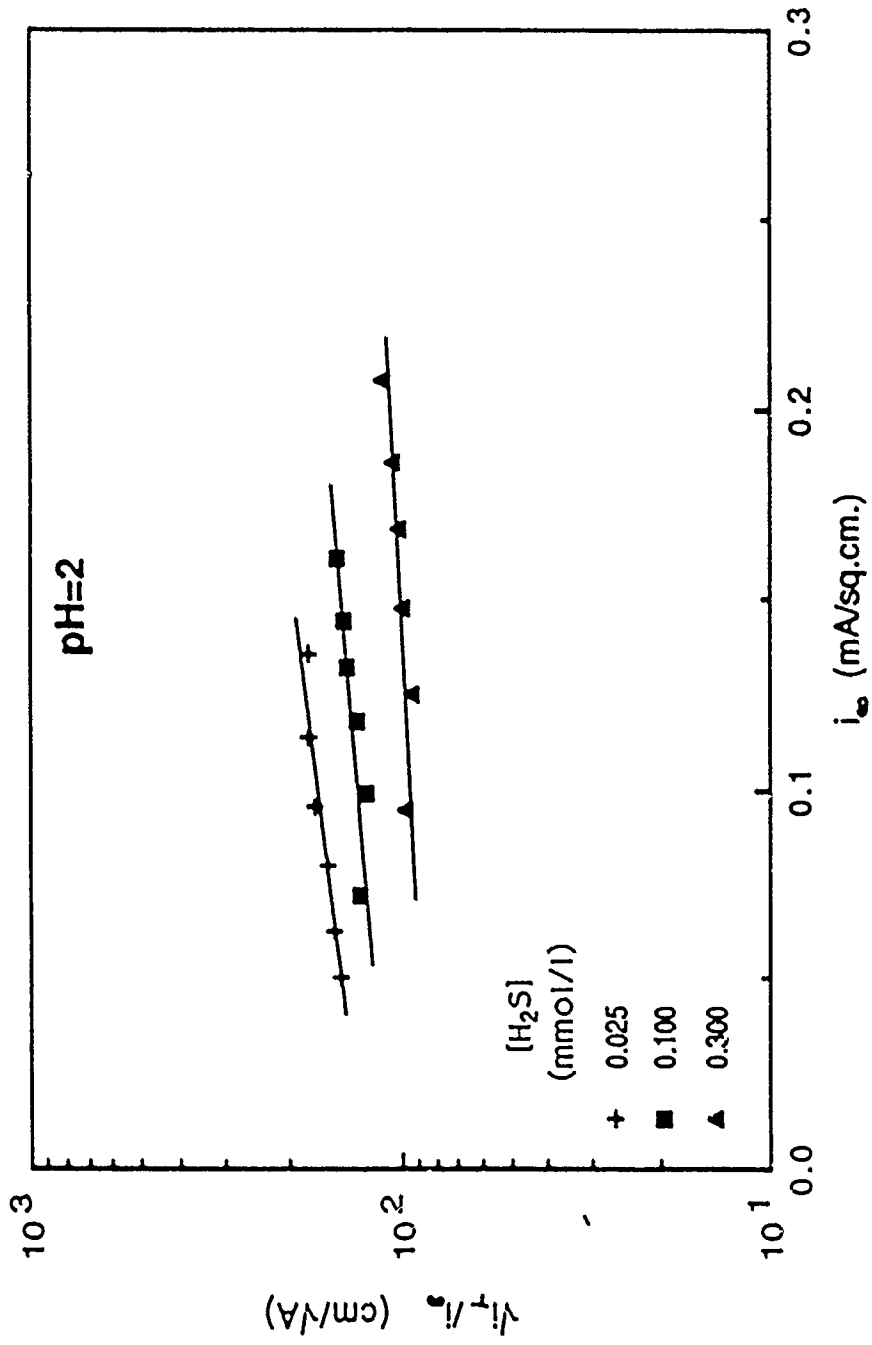


Fig. 7

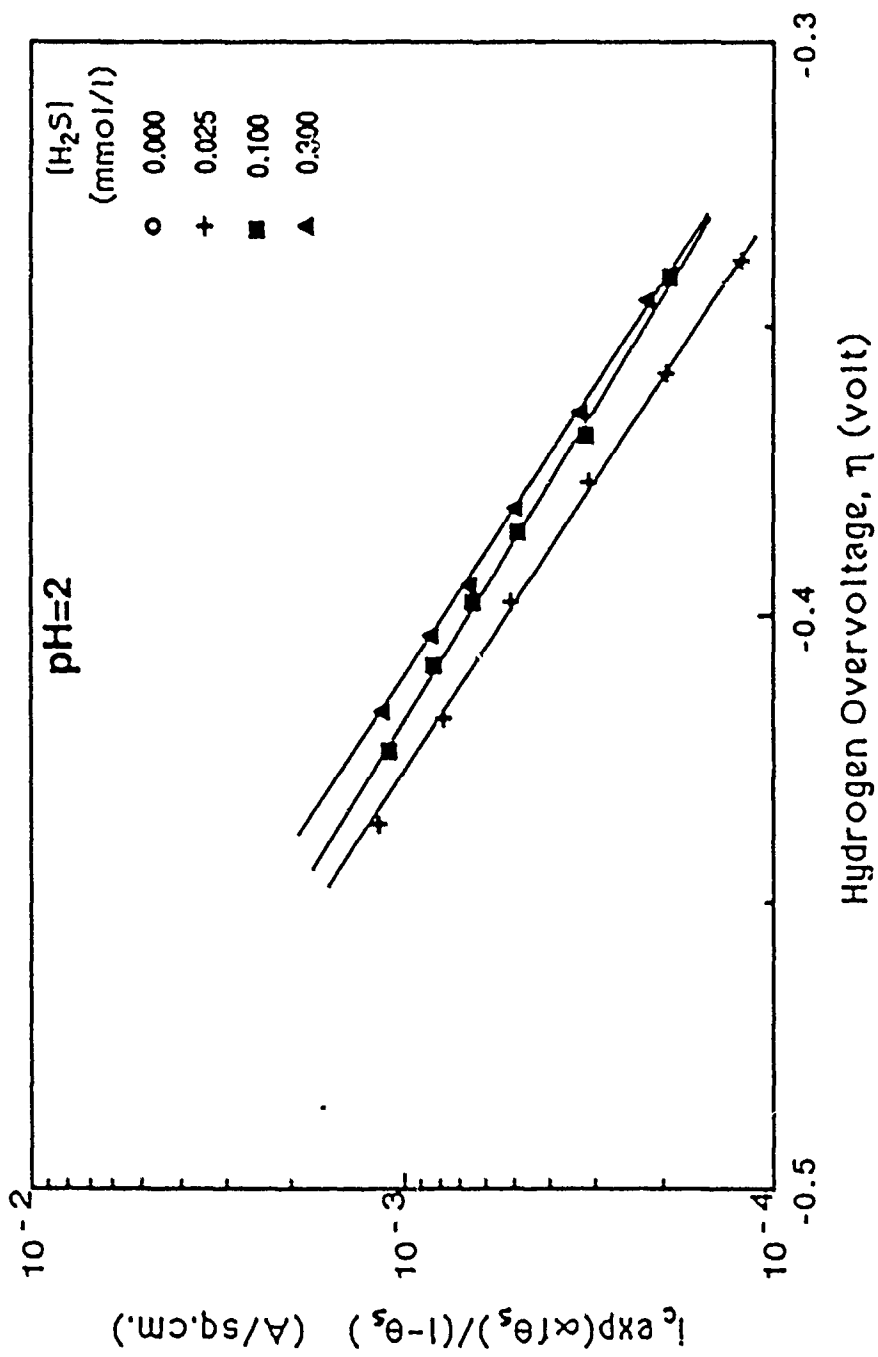


Fig. 8

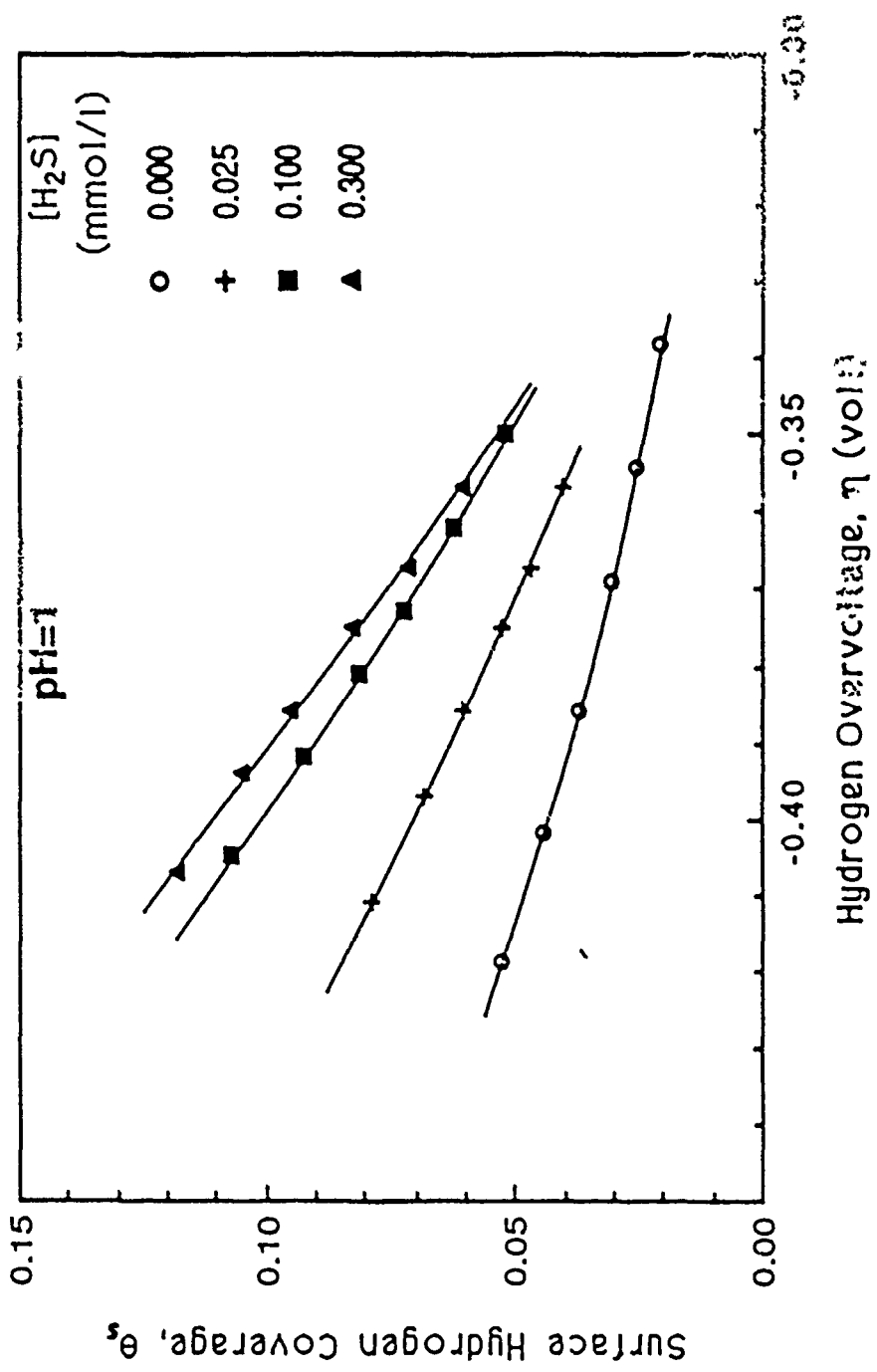


Fig. 9a

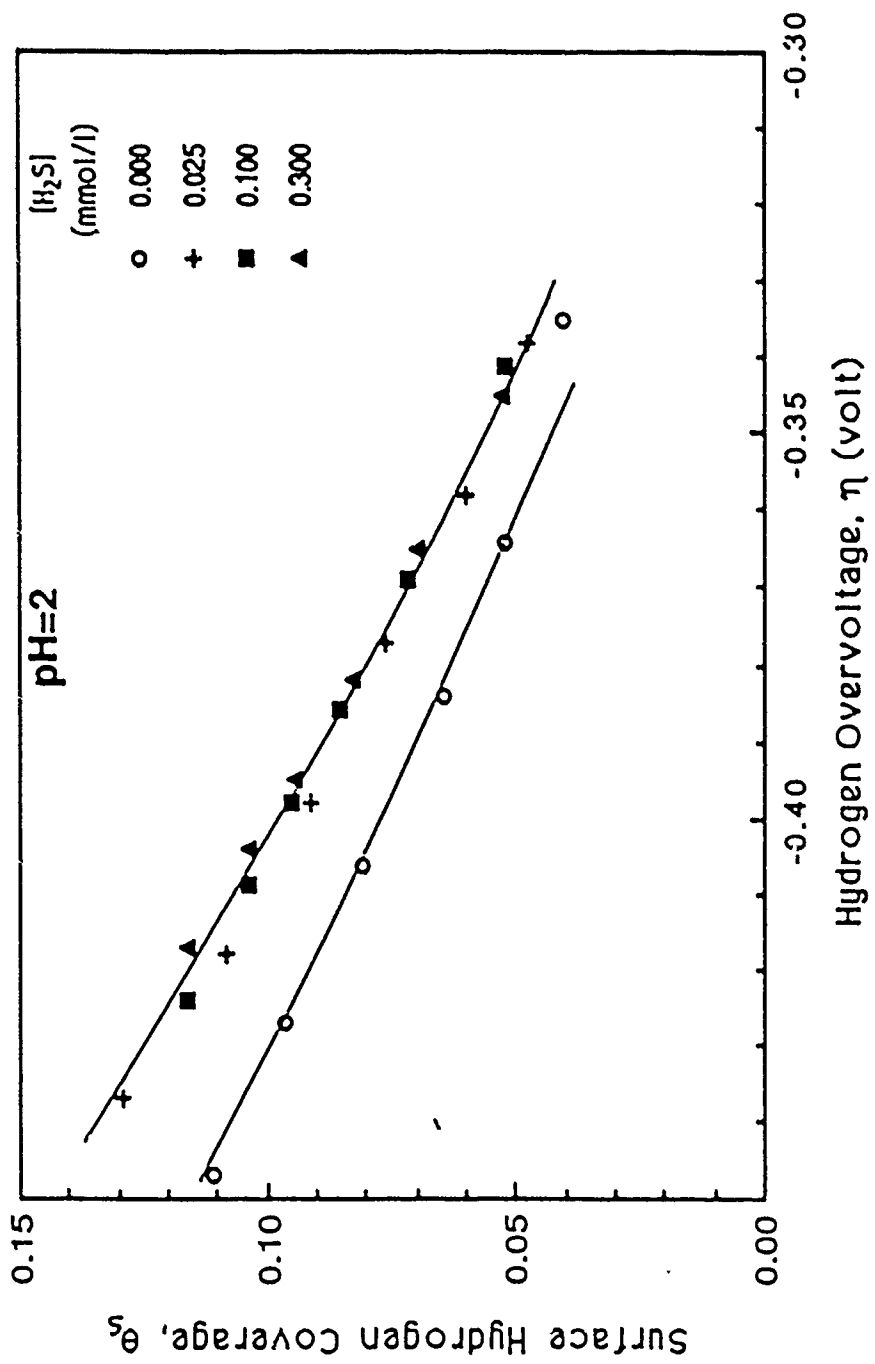


Fig. 9b

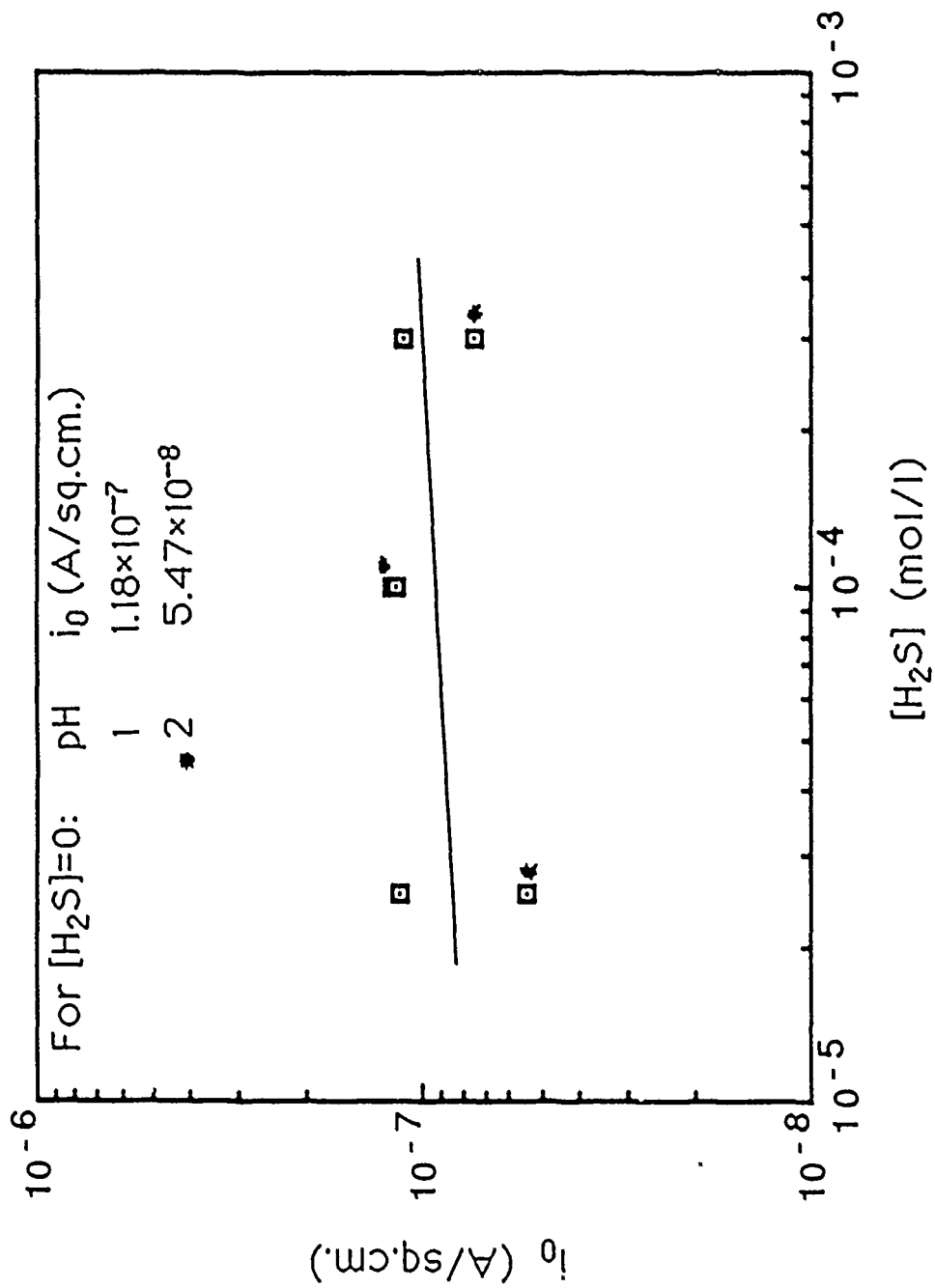


Fig. 10

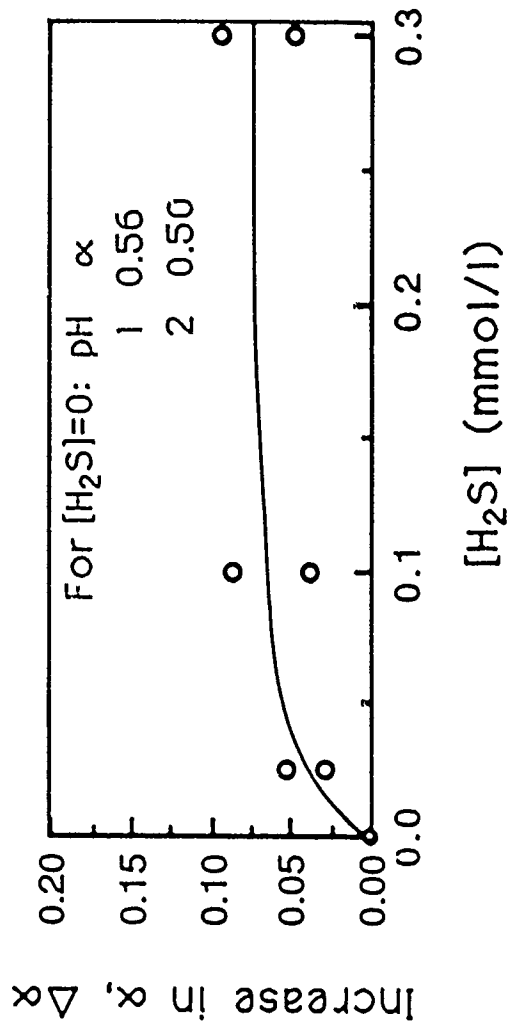


Fig. 11

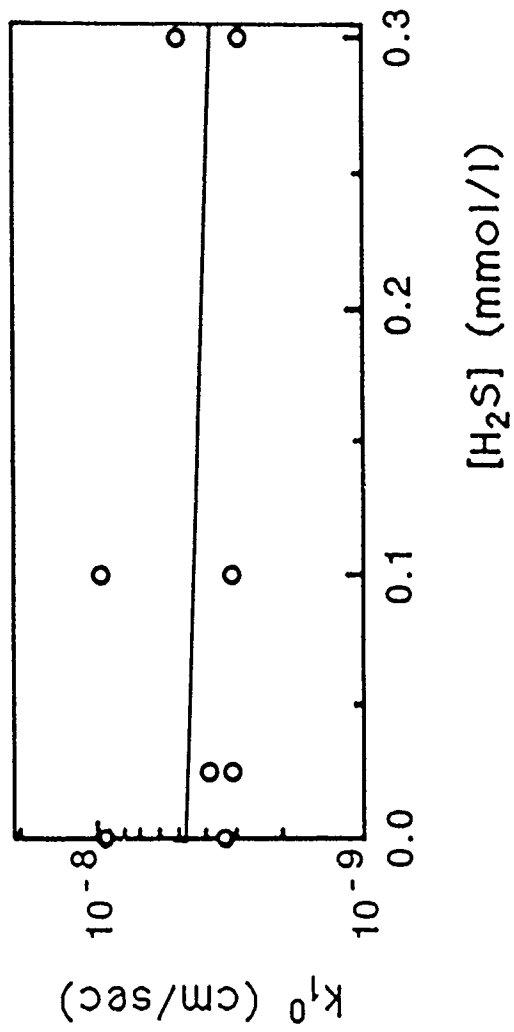


Fig. 12

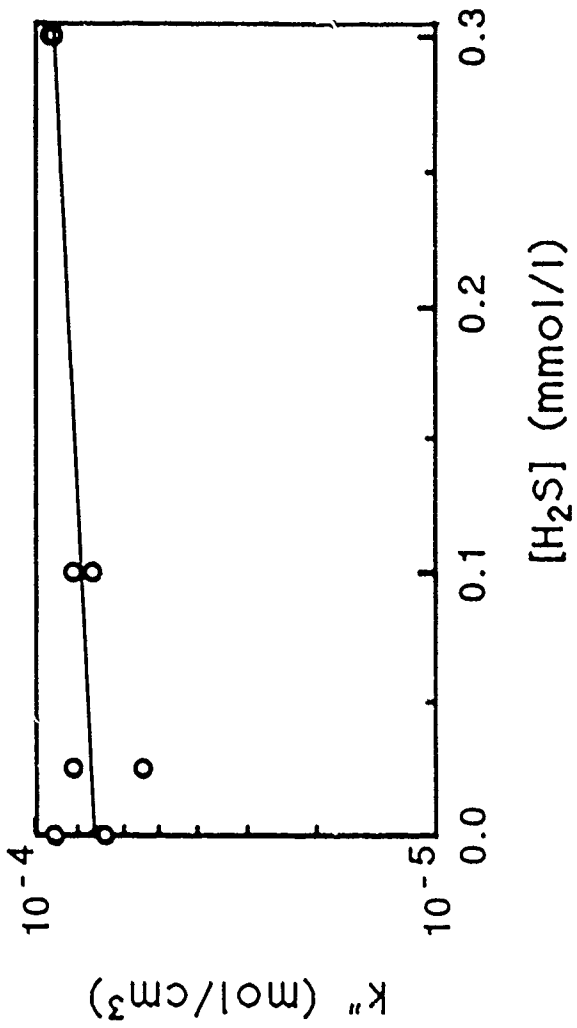


Fig. 13

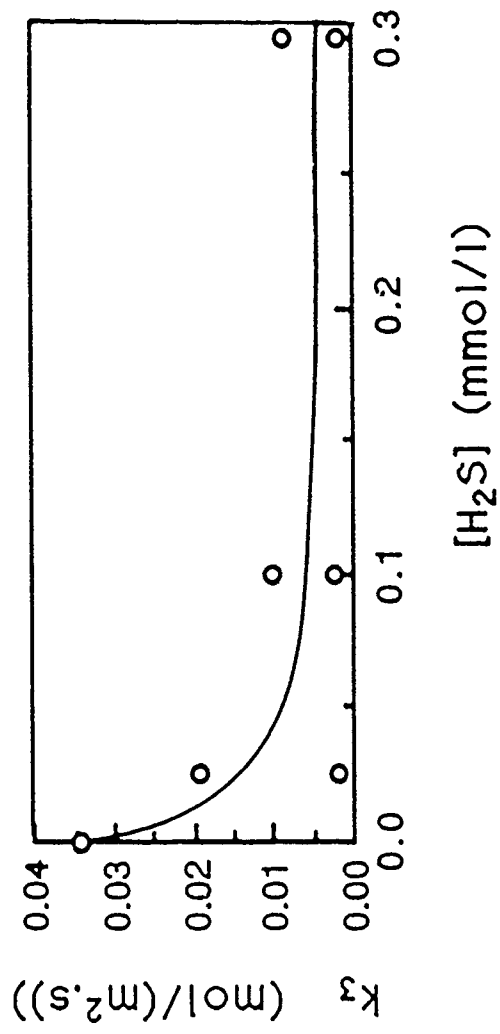


Fig. 14

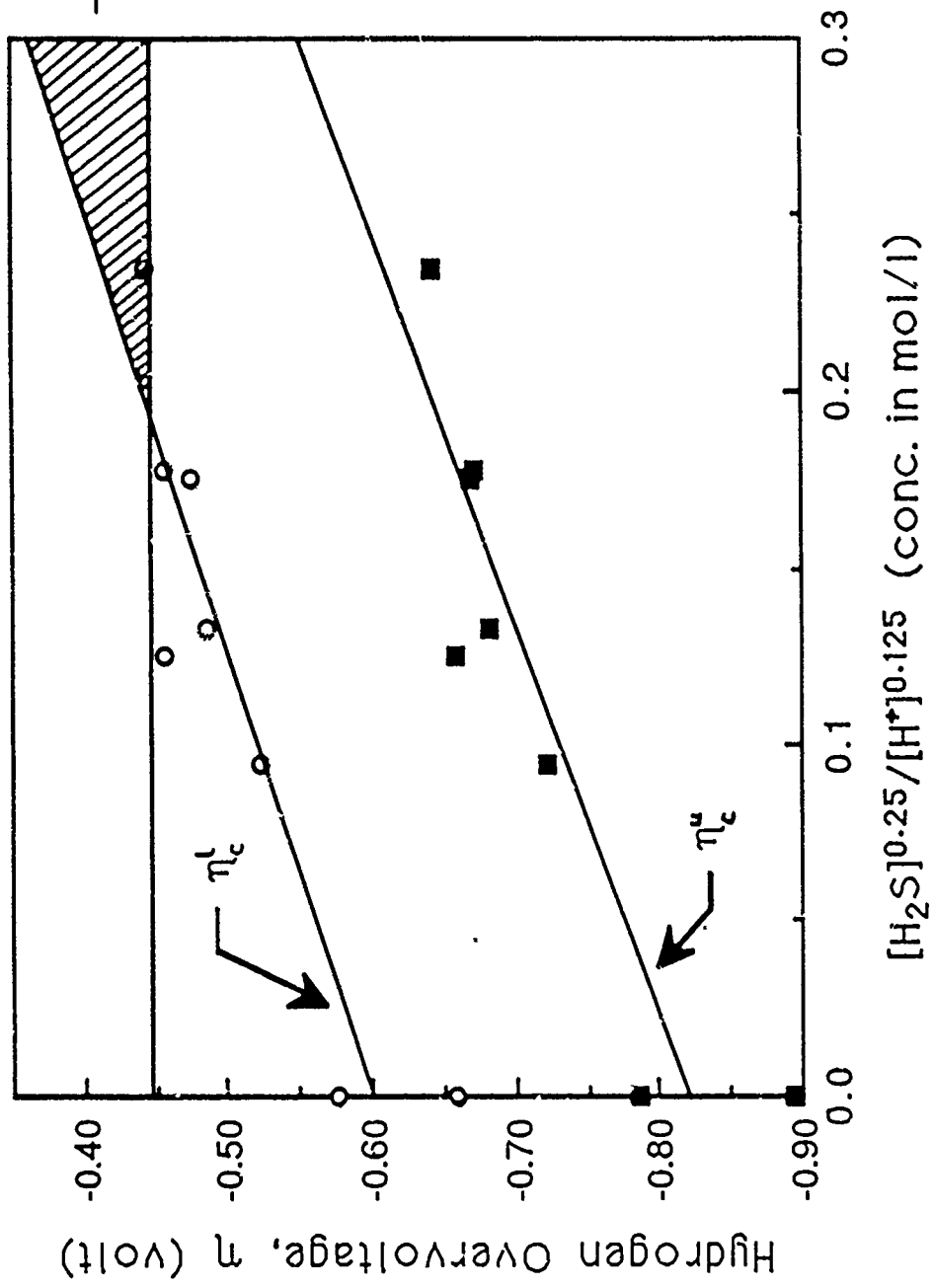


Fig. 15

BASIC DISTRIBUTION LIST

Technical and Summary Reports

1988

<u>Organization</u>	<u>Copies</u>	<u>Organization</u>	<u>Copies</u>
Defense Documentation Center Cameron Station Alexandria, VA 22314	12	Naval Air Prop. Test Ctr. Trenton, NY 08628 ATTN: Library	1
Office of Naval Research Dept. of the Navy 800 N. Quincy Street Arlington, VA 22217 Attn: Code 1131	3	Naval Construction Battalion Civil Engineering Laboratory Port Hueneme, CA 93043 ATTN: Materials Div.	1
Naval Research Laboratory Washington, DC 20375 ATTN: Codes 6000 6300 2627		Naval Electronics Laboratory San Diego, CA 92152 ATTN: Electron Materials Sciences Division	1
Naval Air Development Center Code 606 Warminster, PA 18974 ATTN: Dr. J. DeLuccia		Naval Missile Center Materials Consultant Code 3312-1 Point Mugu, CA 92041	1
Commanding Officer Naval Surface Weapons Center White Oak Laboratory Silver Spring, MD 20910 ATTN: Library	1	Commander David Taylor Research Center Bethesda, MD 20084	1
Naval Oceans Systems Center San Diego, CA 92132 ATTN: Library	1	Naval Underwater System Ctr. Newport, RI 02840 ATTN: Library	1
Naval Postgraduate School Monterey, CA 93940 ATTN: Mechanical Engineering Department	1	Naval Weapons Center China Lake, CA 93555 ATTN: Library	1
Naval Air Systems Command Washington, DC 20360 Attn: Code 310A Code 5304B Code 931A	1 1 1	NASA Lewis Research Center 21000 Brookpark Road Cleveland, OH 44135 ATTN: Library	1
Naval Sea System Command Washington, DC 20362 ATTN: Code 05M Code 05R	1 1	National Bureau of Standards Gaithersburg, MD 20899 Attn: Metallurgy Division Ceramics Division Fracture & Deformation Division	1 1 1

Naval Facilities Engineering
Command
Alexandria, VA 22331
ATTN: Code 03

1

Scientific Advisor
Commandant of the Marine Corps
Washington, DC 20380
ATTN: Code AX

1

Army Research Office
P.O. Box 12211
Research Triangle Park, NC 27709
ATTN: Metallurgy & Ceramics
Program

1

Army Materials and Mechanics
Research Center
Watertown, MA 02172
ATTN: Research Programs Office

1

Air Force Office of Scientific
Research/NE
Building 410
Bolling Air Force Base
Washington, DC 20332
ATTN: Electronics & Materials
Science Directorate

1

NASA Headquarters
Washington, DC 20546
Attn: Code RM

1

Defense Metals & Ceramics
Information Center
Battelle Memorial Inst.
505 King Avenue
Columbus, OH 43201

1

Metals and Ceramics Div.
Oak Ridge National Laboratory
P.O. Box X
Oak Ridge, TN 37380

1

Los Alamos Scientific Lab.
P.O. Box 1663
Los Alamos, NM 87544
ATTN: Report Librarian

1

Argonne National Laboratory
Metallurgy Division
P.O. Box 229
Lemont, IL 60439

1

Brookhaven National Laboratory
Technical Information Division
Upton, Long Island
New York 11973
Attn: Research Library

1

Lawrence Radiation Lab.
Library
Building 50, Room 134
Berkeley, CA

1

David Taylor Research Ctr
Annapolis, MD 21402-5067
ATTN: Code 281
Code 2813
Code 0115

1

1

1

Supplemental Distribution List

Feb 1988

Prof. I.M. Bernstein
Illinois Institute of Technology
IIT Center
Chicago, Ill 60615

Prof. H.K. Birnbaum
Dept. of Metallurgy & Mining Eng.
University of Illinois
Urbana, Ill 61801

Prof. H.W. Pickering
Dept. of Materials Science and Eng.
The Pennsylvania State University
University Park, PA 16802

Prof. D.J. Duquette
Dept. of Metallurgical Eng.
Rensselaer Polytechnic Inst.
Troy, NY 12181

Prof. J.P. Hirth
Dept. of Metallurgical Eng.
The Ohio State University
116 West 19th Avenue
Columbus, OH 43210-1179

Prof. H. Leidheiser, Jr.
Center for Coatings and Surface Research
Sinclair Laboratory, Bld. No. 7
Lehigh University
Bethlehem, PA 18015

Dr. M. Kendig
Rockwell International Science Center
1049 Camino Dos Rios
P.O. Box 1085
Thousand Oaks, CA 91360

Prof. R. A. Rapp
Dept. of Metallurgical Eng.
The Ohio State University
116 West 19th Avenue
Columbus, OH 43210-1179

Prof. G.H. Meier and F.S. Pettit
Dept. of Metallurgical and
Materials Eng.
University of Pittsburgh
Pittsburgh, PA 15261

Dr. W. C. Moshier
Martin Marietta Laboratories
1450 South Rolling Rd.
Baltimore, MD 21227-3898

Prof. P.J. Moran
Dept. of Materials Science & Eng.
The Johns Hopkins University
Baltimore, MD 21218

Prof. J. Kruger
Dept. of Materials Science & Eng.
The Johns Hopkins University
Baltimore, MD 21218

Prof. R.P. Wei
Dept. of Mechanical Engineering
and Mechanics
Lehigh University
Bethlehem, PA 18015

Prof. W.H. Hartt
Department of Ocean Engineering
Florida Atlantic University
Boca Raton, Florida 33431

Dr. B.G. Pound
SRI International
333 Ravenswood Ave.
Menlo Park, CA 94025

Prof. C.R. Clayton
Department of Materials Science
& Engineering
State University of New York
Stony Brook
Long Island, New York 11794

Prof. Boris D. Cahan
Dept. of Chemistry
Case Western Reserve Univ.
Cleveland, Ohio 44106

Dr. K. Sadananda
Code 6323
Naval Research Laboratory
Washington, D.C. 20375

Prof. M.E. Orazem
Dept. of Chemical Engineering
University of Virginia
Charlottesville, VA 22901

Dr. G.R. Yoder
Code 6384
Naval Research Laboratory
Washington, D.C. 20375

Dr. N. S. Bornstein
United Technologies Research Center
East Hartford, CT 06108

Dr. A.L. Moran
Code 2812
David Taylor Research Center
Annapolis, MD 21402-5067

Dr. B.E. Wilde
Dept. of Metallurgical Engineering
The Ohio State University
116 West 19th Avenue
Columbus, OH 43210-1179

Prof. G.R. St. Pierre
Dept. of Metallurgical Eng.
The Ohio State University
116 West 19th Avenue
Columbus, OH 43210-1179

Prof. G. Simkovich
Dept. of Materials Science & Eng.
The Pennsylvania State University
University Park, PA 16802

Dr. E. McCafferty
Code 6322
Naval Research Laboratory
Washington, D. C. 20375

Dr. J.A. Sprague
Code 4672
Naval Research Laboratory
Washington, D.C. 20375

Dr. C.M. Gilmore
The George Washington University
School of Engineering & Applied
Science
Washington, D.C. 20052

Dr. F.B. Mansfeld
Dept. of Materials Science
University of Southern California
University Park
Los Angeles, CA 90089

Dr. Ulrich Stimming
Dept. of Chemical Eng. & Applied
Chemistry
Columbia University
New York, N.Y. 10027

Prof. J. O'M. Bockris
Dept. of Chemistry
Texas A & M University
College Station, TX 77843